A Metrology for Comprehensive Thermoelectric Device Characterization

by

Kelly Lofgreen

A Thesis Presented in Partial Fulfillment
of the Requirements for the Degree
Master of Science

Approved April 2011 by the
Graduate Supervisory Committee:

Patrick Phelan, Chair
Jonathan Posner
Shankar Devasenathipathy

ARIZONA STATE UNIVERSITY

May 2011

ABSTRACT

Thermoelectric devices (TED's) continue to be an area of high interest in both thermal management and energy harvesting applications. Due to their compact size, reliable performance, and their ability to accomplish sub-ambient cooling, much effort is being focused on optimized methods for characterization and integration of TED's for future applications.

Predictive modeling methods can only achieve accurate results with robust input physical parameters, therefore TED characterization methods are critical for future development of the field. Often times, physical properties of TED sub-components are very well known, however the "effective" properties of a TED module can be difficult to measure with certainty. The module-level properties must be included in predictive modeling, since these include electrical and thermal contact resistances which are difficult to analytically derive.

A unique characterization method is proposed, which offers the ability to directly measure all device-level physical parameters required for accurate modeling. Among many other unique features, the metrology allows the capability to perform an independent validation of empirical parameters by measuring parasitic heat losses. As support for the accuracy of the measured parameters, the metrology output from an off-the-shelf TED is used in a system-level thermal model to predict and validate observed metrology temperatures.

Finally, as an extension to the benefits of this metrology, it is shown that resulting data can be used to empirically validate a device-level dimensionless relationship. The output provides a powerful performance prediction tool, since all physical behavior in a performance domain is captured using a single analytical relationship and can be plotted on a singe graph.

TABLE OF CONTENTS

Page

LIST OF TABLES vi

LIST OF FIGURES vii

LIST OF SYMBOLS / NOMENCLATURE viii

CHAPTER

1 INTRODUCTION 2

2 BACKGROUND 7

2.1 Thermoelectric Phenomena 7

2.2 Physics of a Single Thermoelectric Couple......................9

2.3 Module-Level Analysis 17

2.3.1 Voltage Components.......................................18

2.3.2 Input Power Components................................19

2.4 Characterization Methods 20

2.5 Modeling Methods 29

3 EMPIRICAL CHARACTERIZATION....................................... 34

3.1 Metrology Overview..34

3.2 Accuracy Evaluation 38

3.3 Extrapolation to Face Temperatures..............................43

3.4 Measurement Results 47

3.4.1 Thermal Resistance Measurement 47

3.4.2 Module Seebeck Coefficient Measurement 48

3.4.2 Electrical Resistance Measurement.................51

3.5 Empirical Validation of Measured Parameters 54
4 MODELING 56
4.1 Model Overview 56
4.2 Modeling Results 63
4.3 Buckingham Pi Analysis 71
5 CONCLUSION 80
REFERENCES 84

LIST OF TABLES

Table Page

1. Physical Phenomena in Thermoelectric Devices...................... 8

2. Metrology Inputs and Affect Quantities 37

3. Metrology Outputs and Associated Quantities........................ 38

4. Temperatures Measured in Metrology Accuracy Evaluation .. 43

5. Heatflow Calculation Results per Measurements from Thermocouples in the Upper and Lower Aluminum Blocks…………………………………………………………… 43

6. Summary of Thermal Ressitances of the Substrate and Interconnect Layers 46

LIST OF FIGURES

Figure Page

1. Typical Performance Criteria Reported by Manufacturers......... 6

2. Single Thermoelectric Couple 10

3. Evolution of the ZT Figure of Merit 16

4. Thermoelectric Device Module Schematic 18

5. Applied Current and Voltage Response Using the Harman Method 24

6. Assumed versus Actual Configurations Under Some Test Methods 24

7. Foster and Cauer Network Modeling Schematics.................. 31

8. Metrology Schematic With Thermocouple Locations 36

9. Metrology Schematic 36

10. Metrology Temperatures Measured for Accuracy Evaluation .. 40

11. Temperatures Measured in the Aluminum Blocks 40

12. Thermal Resistance Stack-up 45

13. Thermal Resistance versus Temperature 49

14. Module Seebeck Coefficient versus Temperature 50

15. Electrical Resistance versus temperatures 53

16. Correlation Between Measure Power and Computed Power for Experiments used to Generate Parameters 55

17. Correlation Between Measured Power and Computed Power for Independent Test Conditions 55

18. Schematic of System-level Metrology Thermal Network Model,
Overlaid with Physical System Schematic 58
19. Electrical Network Schematic of the Metrology System-level
Thermal Model 58
20. Schematic of the Sub-system Thermal Network Model Overlaid
with a Physical System Schematic 60
21. Electrical Network Schematic of the Sub-system 62
22. Numbered Physical Locations Used in Model Matching.......... 64
23. Model Output and Metrology Temperatures for the Baseline
Case, 0A Current Applied 65
24. Model Output and Metrology Temperatures for the Baseline
Case, 2A Current Applied 66
25. Model Output and Metrology Temperatures for the Baseline
Case, 4A Current Applied 66
26. Model Output and Metrology Temperatures for the Baseline
Case, 6A Current Applied 67
27. Model Output and Metrology Temperatures for the Baseline
Case, 8A Current Applied 67
28. Model versus Experimental Data for Power Through the Lower
Aluminum Block 69
29. Model versus Experimental Data for Power Through the Upper
Aluminum Block 71

30. Simple Thermoelectric System 73

31. Schematic of a Simple Thermoelectric System with All Relevant Physical Parameters 73

32. Simplified Thermoelectric System Shown with Independant Parameters Only 75

33. Dimensionless Parameter Experimental Fit with that Predicted by the Developed Buckingham Pi Model........................... 77

34. Experimental Fit of Control-side Temperature with that Predicted by the Developed Buckinham Pi Model............................ 77

35. Dimensionless Parameter Contour Plot of the Developed Buckingham Pi Model 78

36. Contour Plot of Control-side Temperature as Predicted Using the Developed Buckingham Pi Model 79

LIST OF SYMBOLS

A, area

C, thermal capacitance

COP, Coefficient of Performance

I, current

K, thermal conductance

P, electrical power input

Q, heat flow

R^2, Coefficient of Determination

R_j, electrical Resistance

R_{th} , thermal resistance

T, Temperature

V, Voltage

Z, TED figure of Merit

l, thicknes

k, thermal conductivity

n, number of thermoelectric couples in a TED module

α, Seebeck Coefficient

ρ, Electrical resistivity

ΔT, Temperature difference across the TED

dT/dx, derivative of temperature with respect to length

1. INTRODUCTION

Thermoelectric devices (TEDs) represent an area of huge interest in thermal management and energy harvesting. For Example, the the U.S. Department of Energy is actively funding research in advanced automotive waste heat applications, with the goal of improving fuel economy by up to 15% by the year 2020 [1]. Arguable the most pressing demand in the area of thermal management is from manufacturers of laser diodes for optical communication. According to the latest forecast report by LightCounting, sales of optical transceivers increased by 35% in 2010, and is expected to continue with strong growth [2]. With the increased levels of demand, TED manufacturers will continue to develop thermoelectric technologies to be smaller and more efficient. The two main areas of use include temperature control, and power generation. TED's can be operated in two states; either in a power generation mode, or a temperature control mode, described below:

- Electrical power generation. Via the Peltier effect, a temperature difference across a TED results in an emf, and when an electrical load is connected in series, an electrical work output can be derived.
- Electrical power input to achieve a desired temperature or heat flow on the control-side of the TED. Work in the form of electrical power can be input to the TED, resulting in a temperature difference and heat flow.

Many of the physical relationships discussed here are applicable to TEDs used in both configurations described above, however, since the aim of this work is to analyze TEDs for use in cooling application, we will present the analysis

from this perspective. Current uses for TEDs include refrigeration devices, such as air conditioners and small coolers, personal comfort, and cooling of temperature-sensitive electronics [3-5]. For the current and future applications, the use of TEDs in thermal management is extremely attractive. Among other advantages, TEDs have no moving parts which lend to good reliability, and almost non-existent maintenance. The technology is highly scalable, with currently available sizes ranging from the order of 30 square centimeters [6] to as small as 4 square millimeters [7]. The development of sputtered and superlattice thermoelectric materials has enabled TEDs as thin as 100μm [8]. As a thermal management technology, TEDs offer the capability to refrigerate, that is, cool to temperatures below ambient temperature. Fan-sinks and passive heat-sinks are limited fundamentally by the fact that they cannot cool to temperatures lower than that of the ambient, no matter how low the effective thermal resistance of the thermal solution. A number of different refrigeration technologies are reviewed in [9], and from the study it was found that, as of 2001, TEDs were the only commercially available technology for miniature refrigeration. With the recent advancements in miniaturization, TEDs are only becoming a more suitable option for small-scale cooling. Perhaps one of the most exciting applications for TEDs is for the use of localized, on-demand cooling of CPU high power-density regions. A necessary component of effective CPU thermal management requires a package-level spreading of the high heat flux regions on the CPU [10]. Miniature TED's represent a potential solution for achieving package-level thermal

management in an environment where CPU transistor density is growing at exponential rates [11].

Another area of growing demand for TED’s is in the area of precision temperature control. The expanding infrastructure of fiber optics and laser diodes has emerged as a huge area of demand for to TED’s, as they are one of the few options for controlling temperature to within fractions of a degree. Since laser diodes which source light in optical transceivers are sensitive to the ambient temperature, TED’s, along with a precision controller, can achieve the desired control state. Some applications require control to within 0.1K of an optimal working temperature [12]. It is no doubt that demand will continue to increase for TED’s in this application.

Because of the highly non-linear behavior of TED’s, and the number of variables involved, achieving accurate performance prediction often requires a thermal model of the TED system. This is especially the case for systems involving three-dimensional effects, such as heat spreading and/or non-uniform power. Typically, TED suppliers do not facilitate the information necessary to achieve performance prediction in a thermal model. Information released by suppliers for TED models typically includes performance curves such as (1) heat pumped vs. temperature difference across the TED, and (2) power input to the TED vs. temperature difference across the TED. Examples of these metrics for a standard TED module can be seen in Figure 1. These curves are enough to perform an extremely “high-level” analyses to find a suitable TED, however they cannot be input to a detailed thermal model to predict performance.

The motivation for the developed metrology addresses two main areas of need. First, the solution offers a method by which designers can extract information needed to predict performance in a detailed thermal model. Second, the solution can be used by TED manufacturers to both guage and communicate applicable metrics to show performance and performance improvements.

The objective of this thesis will be to present a unique test method which offers many advantages over existing methods, and which has the ability to capture all relevant thermo-physical parameters and their temperature dependence required to predict performance in a thermal model. To offer support of this claim, it will be shown that parameters can be directly used in a thermal model to give a match in temperature with that observed.

Finally, utilizing one of the unique benefits of the metrology (namely, that the TED can be operated and tested at use-condition input currents) a non-dimensional analysis will be performed. It will be shown that the output from the particular analysis can offer a concise tool by which designers can predict performance of a TED in a simple system.

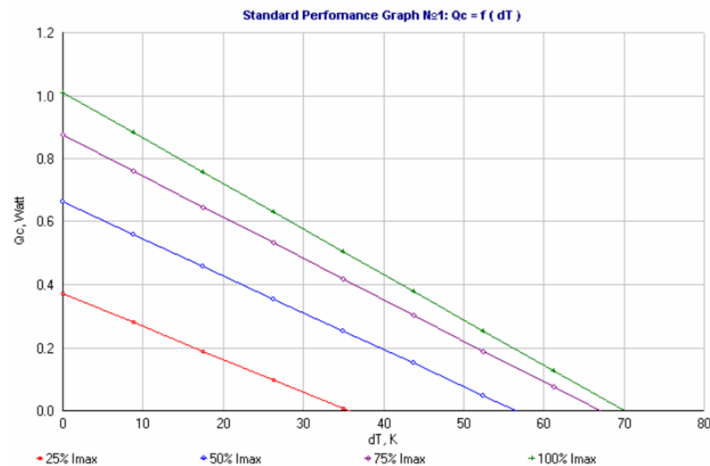

a) Heat pumped vs. temperature difference for various current levels.

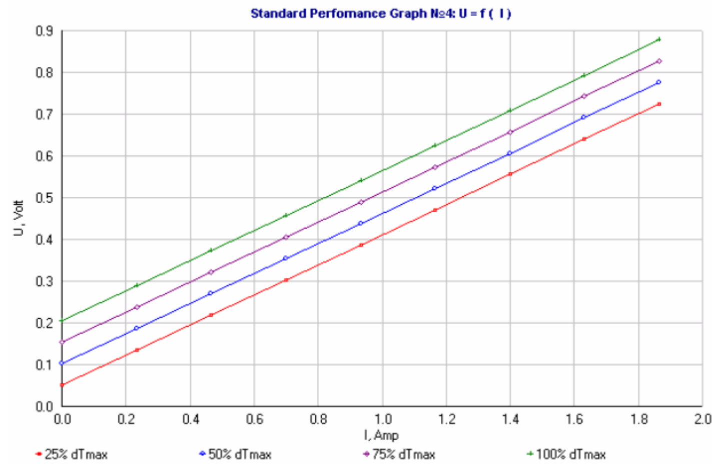

b) Current and voltage (i.e. power) for various temperature difference

Figure 1-Example of a typical manufacturer TED performance metric[13].

2. BACKGROUND

2.1 Thermoelectric Phenomena

In one of his most famous works, Peltier showed that heat is liberated or absorbed when an electric current crosses a boundary composed of dissimilar conductors [14]. The heat liberated or absorbed at the interface is a result of the entropy change of the charge carriers as they move across the interfaces. This phenomenon, known as the Peltier effect, is one of three fundamental mechanisms which form the basis of function in a TED. The other two phenomena are called the Thompson effect and the Seebeck effect. The Thompson effect is a bulk material effect, which occurs when heat is liberated or

absorbed as current flows through a single conductor subject to a temperature gradient. The Seebeck effect, also a bulk material effect, is characterized by the formation of a voltage in a conductor subject to a temperature gradient. It is important to note that the Seebeck effect, unlike the Peltier and Thompson effects, is applicable under open-circuit conditions (i.e. no current flow) as well as closed circuit conditions (i.e. current flow present). All three effects are also reversible, that is, zero net entropy change results from the Peltier, Seebeck, and Thompson effects. Table 1 summarizes the three effects.

Table 1-Physical Phenomena in Thermoelectric Devices.

Physical Effect	**Location of occurance**	**Applicabile when**
Peltier	Surface	$\|I\| > 0$
Seebeck	Volume	$\|I\| \geq 0$
Thompson	Volume	$\|I\| > 0$

Though the phenomena described here are well understood, a complete explanation is highly complicated and requires an understanding of both quantum mechanics and thermodynamics. Detailed explanations will not be covered in this paper, but can be found in texts such as The CRC Handbook of Thermoelectrics [15] .

Due to the closely related nature of the three effects, a material property known as the Seebeck Coefficient can be used to characterize them in a material[15]. As in the case of the Peltier effect – since this effect involves the interface between two materials – the Peltier cooling and heating can be described by the difference of the material Seebeck coefficients. The Seebeck coefficient is typically higher in semiconductors than in metallic conductors, though the resistivity is also higher in semiconductors. The material resistivity contributes to an irreversible Joule heating effect in a TED. In a TED, it is desirable to choose TE element materials which have high absolute values of the Seebeck coefficients, since more Peltier heating and cooling results. P-type thermoelectric materials are chosen with a positive Seebeck Coefficient, and n-type thermoelectric materials are chosen with a negative Seebeck Coefficient. This is due to the requirements that the p and n couples are connected in series, and heating and cooling must take place on the same side of the device for a given current flow direction.

When a TED is used as a temperature-control device, it can be operated in a heating or cooling mode, where the mode is dictated by the direction of current through the device. Because the orientation is fixed in a given design, one side of the TED is termed the "control" side, and the opposing side is referred to as the "sink" side. The control side of the TED can accomplish either heating or cooling by altering the current direction. Typically, a PID controller is implemented to achieve the desired control-side temperature by altering the current. For example, when a TED is used for refrigeration, the component to be

cooled is placed close to the control-side of the TED for heat removal, and a heat sink is used to remove the heat dissipated from the sink side.

2.2 Physics of a Single Thermoelectric Couple

Figure 2 shows a schematic of a conceptual TED with only one couple. In the depicted scenario, the simplified TED is operating in cooling mode configuration, with the control side of the TED absorbing heat and placed close to the object being thermally managed (in this case, it is being cooled).

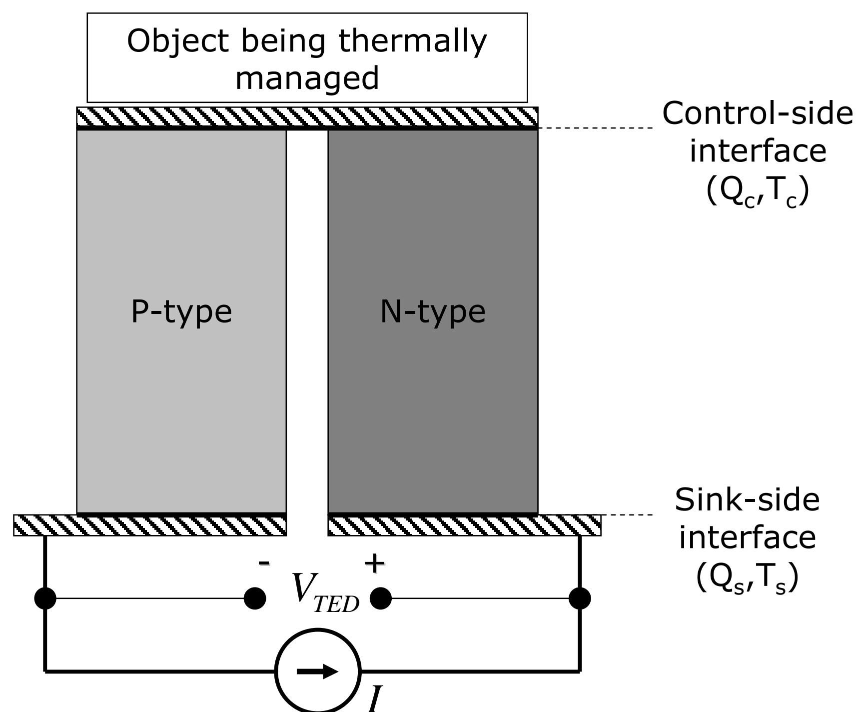

Figure 2-A Single p-type and n-type thermoelectric couple.

Current flow is assumed positive when it flows from a high voltage (positive) to a low voltage (negative), and is consistent with the direction of flow of positive charge carriers. In the configuration shown in Figure 2, the current direction is

counter-clockwise, with the n-type semiconductor connected to high-voltage (positive) side of the current source, and the p-type semiconductor connected to the low-voltage (negative) side of the current source. The diagram includes terms describing the relevant energy exchanges within the TE couple, namely, those which occur at the sink-side and control-side interfaces. The quantity Q_c describes the net heat-flow absorbed at the control-side interface, and the quantity T_c is its absolute temperature. For simplicity, we assume that heat-flow is only in the vertical (up or down) direction. The quantities Q_s and T_s represent the heat flow liberated and the absolute temperature, respectively, at the sink interface. Electrical interconnects exist at each side of the p-type and n-type semiconductors. Typically these are made of copper due to the material's low electrical resistivity and higher thermal conductivity. The function of the electrical interconnects is only to electrically couple the p-type and n-type semiconductors.

In addition to the Peltier effect, there are two additional effects which must be considered. These additional effects are irreversible, and often are the primary cause of any loss in efficiency of a TED:

- Joule heating – both a volumetric and interfacial heating effect, which depends on the electric current and resistance (both bulk and contact) of the TED.
- Internal heat conduction – heat conduction through the TE elements due to the temperature difference of the control and sink sides of the TED.

Equations presented in this chapter are a result of an energy balance analysis, considering conduction, Joule heating, and the Peltier effect within a

single thermoelectric couple, as shown in Figure 2. To simplify the analysis, certain assumptions are made. The main assumptions are listed below:

- 1D heat conduction, adiabatic lateral surfaces
- Isothermal sink-side and control-side interfaces
- Constant properties over the length of the elements (Seebeck Coefficient, electrical conductivity, and thermal conductivity),
- Constant Seebeck coefficient implies that the Thompson effect is ignored.

It should be noted that the assumption of constant properties does not exclude the option to consider the properties' variation with temperature. Neglecting the variation of properties over the length of the elements should in no way imply that the property temperature dependence is omitted. Omitting the properties' temperature dependence can introduce significant error in the results. For metals, the Seebeck coefficient has been reported to vary by 5-10% over as little as 30℃ [16]. Since the Peltier heat absorbed at the control-side interface is directly proportional to this parameter, any error in this parameter can significantly influence system temperatures.

An analytical expression can be derived based on a surface energy balance at the interface (sink or control side), and based on the heat diffusion equation, solved over the length of the TE elements. Based on the configuration in Figure 2, the resulting equation which quantifies the heat absorbed (cooling power) at the control side interface of the p-n TE couple is given by Equation (2) [17]:

$$Q_c = (\alpha_p - \alpha_n) I T_c - K_{th,s}\left(T_s - T_c\right) - \frac{I^2 R_{j,s}}{2} \quad (2)$$

where α_p and α_n are the Seebeck Coefficients of the p-type and n-type semiconductor elements, respectively, T_c and T_s are the absolute temperatures of the control-side and sink-side interfaces, respectively, $K_{th,s}$ the effective conductance of both p-type and n-type semiconductors, I the applied current, and $R_{j,s}$ the total electrical resistance of both the p-type and n-type semiconductors. Similarly, the equation describing the heat liberated from the sink side interface is given by Equation (3) [17]:

$$Q_s = (\alpha_p - \alpha_n) I T_s - K_{th,s}\left(T_s - T_c\right) + \frac{I^2 R_{j,s}}{2} \quad (3)$$

Where Q_s is the heat liberated by the sink side of the TED. It is evident from Equation (2) that the Peltier cooling (first term) must overcome heat from the TED sink-side (back conduction, second term) and half the Joule heating (third term) for a net positive heat absorbed at the control-side of the TED. The expression also shows that half the Joule heat arrives at the control side interface, while the other half arrives at the sink-side interface. The equations reveal a number of important facets of the Peltier effect. The first thing to note is that the Peltier heat absorbed or liberated depends on the local absolute temperature. It is this dependence which makes the solution to a thermal problem involving TEDs non-trivial. When solving an energy balance for temperatures, if temperature-dependent heat-flow terms are present, an iterative solution is required. Another important learning from these equations is that since the absolute temperature in each equation is different, the Peltier heating is

un-balanced between the control and sink sides – essentially the amount of heat absorbed at the control-side is not the same as the amount dissipated at the sink side. The imbalance is fully accounted for by the Seebeck voltage generated as a result of the temperature difference.

From Equation (2) and Equation (3), a number of additional metrics can be derived. For example, differentiating Equation (2) with respect to I and setting the result equal to zero yields an expression for I_{max}, given by Equation (4) [17]:

$$I_{\max} = \frac{(\alpha_p - \alpha_n)T_c}{R_{j,s}} \tag{4}$$

where I_{max} is the current at maximum control-side heat flow. By substitution of Equation (4) back into Equation (2), we arrive at an expression for the maximum control-side heat flow, which is given by Equation (5) [17]:

$$Q_{c,\max} = \frac{(\alpha_p - \alpha_n)^2 T_c^2}{2R_{j,s}} - K_{th,s}(T_s - T_c) \tag{5}$$

where $Q_{c,max}$ is the maximum control-side heat flow. Equation (5) Reveals the trade-off between the sink and control side temperature difference and the maximum cooling power. The maximum temperature difference can be determined by setting Eqation (5) equal to zero and solving for the maximum temperature difference. The resulting equation is given by Equation (6) [17]:

$$(T_s - T_c)_{\max} = \Delta T_{\max} = \frac{(\alpha_p - \alpha_n)^2 T_c^2}{2K_{th,s}R_{j,s}} \tag{6}$$

where $\Delta T_{max} = (T_s\text{-}T_c)_{max}$ is the maximum temperature difference which can be achieved across the TED. In terms of material properties, we can define a figure

of merit for a TE couple which is proportional to ΔT_{max}. The expression defining the figure of merit for a thermoelectric couple is given by equation (7) [17]:

$$Z = \frac{(\alpha_p - \alpha_n)^2}{K_{th,s} R_{j,s}} \qquad (7)$$

Where Z is the figure of merit for a thermoelectric couple. A higher Seebeck coefficient implies more desired Peltier heat and cooling. A lower thermal conductivity and electrical resistance imply less internal heat conduction, and lower amounts of Joule heating, respectively. Since the figure of merit is also defined for individual materials, it can be used as an indication for the suitability if a material in a thermoelectric device. Since all properties in the Z figure of merit are temperature-dependent, often Z is multiplied by the absolute temperature at which the properties are evaluated. Multiplying by temperature makes the figure of merit non-dimensional. In general, for any given material, the non-dimensional figure of merit is given by Equation (8) [18]:

$$ZT = \frac{\alpha^2}{\rho k} T \qquad (8)$$

where T is the absolute temperature, α the material Seebeck Coefficient, ρ the material resistivity, and k the material thermal conductivity. It should be noted that the extension of a quantity describing a thermoelectric p-type and n-type material to a single material holds the assumption that $\alpha_p = -\alpha_n = \alpha$, *and* $\rho_n k_n = \rho_p k_p = \rho k$. Fortunately, this situation holds for many of the common materials used in thermoelectric refrigeration at ordinary temperatures [19].

Since about 1970, the highest ZT's reported had been around ZT=1 with very little improvement until around the mid 1990's. Over the last 10 years, there has been extensive research into newly developed nanostructured materials, which are engineered for optimal electron and phonon transport for high ZT. To date, the highest ZT reported is around 2.5 [18]. Figure 3 shows a sampling of common thermoelectric materials.

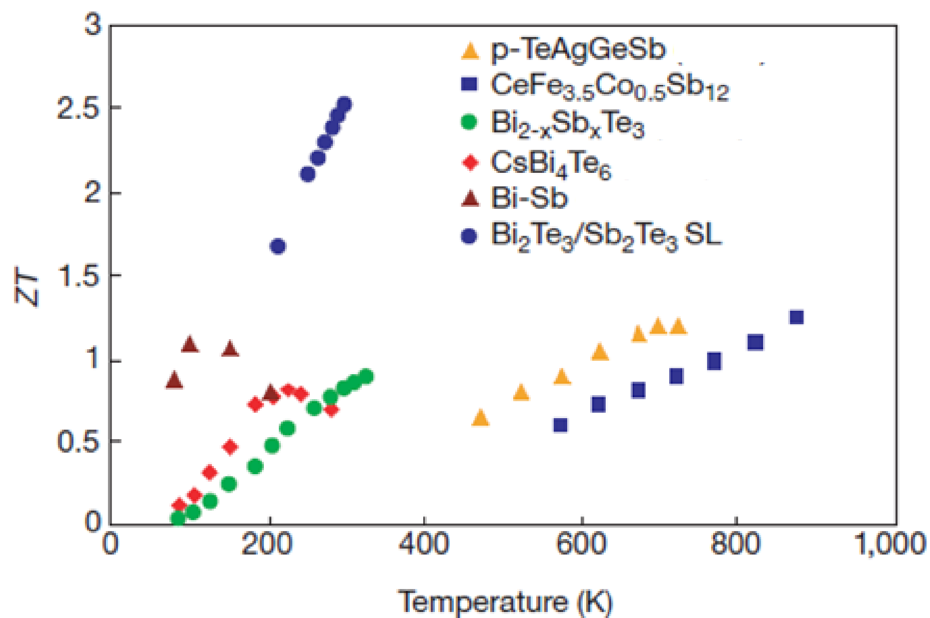

Figure 3-ZT figure of merit in some common thermoelectric materials[18].

Shown in Figure 3 are some of the more commonly used bulk materials ($Be_{2-x}Sb_xTe_3$) as compared with some of the recent nanostructured materials (Be_2Te_3/Sb_2Te_3SL). There is no theoretical upper limit to ZT, and it is thought that above ZT=3, thermoelectric refrigeration will become comparable in performance to vapor compression systems [20].

2.3 Module-Level Analysis

Many of the relations discussed for a single couple apply to the device-level analysis. Simply put, a TED is nothing more than many TE couples connected in series. For a given current, the heat absorbed on the TED control-side is proportional to the number of couples in a TED. Figure 4 shows a detailed TED schematic. As labeled in the figure, the main components are the dielectric substrates (usually ceramic), the electrical interconnect conductors (usually copper), and the p-type and n-type semiconductor thermoelectric elements. The substrate and interconnects exist only as support structures and electrical connections, respectively, for the thermoelectric elements. Because the Peltier cooling is purely additive over the number of thermoelectric p-n couples, Equation (2) can be extended to represent device-level heat flow equations. The result is given by Equation (9) [21]:

$$Q_c = n\left[(\alpha_p - \alpha_n)IT_c - K_{th,s}\left(T_s - T_c\right) - \frac{I^2 R_{j,s}}{2}\right] \tag{9}$$

where Q_c represents the total heat absorbed at the control side of the TED, and n the number of thermocouples. A similar equation applies to the heat liberated on the sink side of the TED.

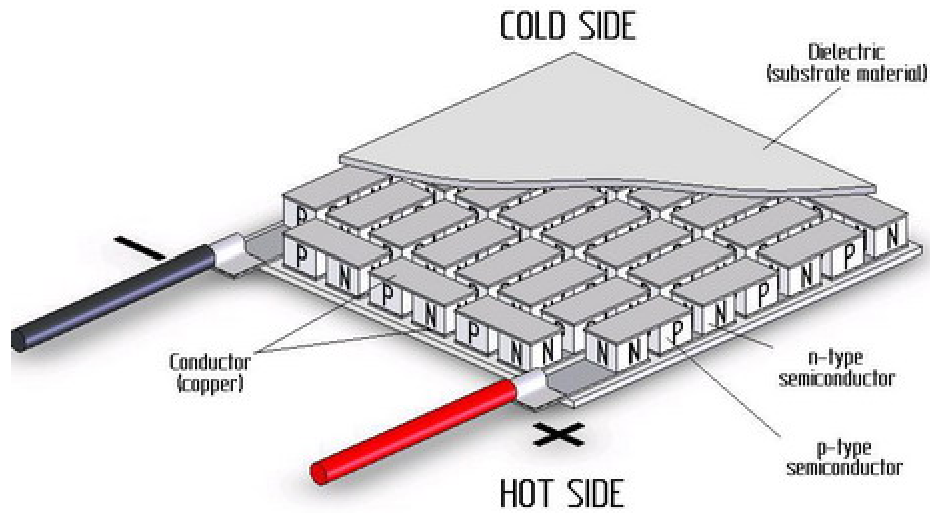

Figure 3-TED module schematic [22].

2.3.1 Voltage Components

It is important to understand the components of input power for a TED. Before this, the input voltage components must be discussed. When a current is applied to a TED, the corresponding voltage which can be measured across the TED can be divided into two terms, namely the Joule voltage and the Seebeck Voltage. The simple expression is given by

$$V_{TED} = V_J + V_\alpha \qquad (10)$$

where V_J is the Joule voltage component, V_α the Seebeck voltage component, and V_{TED} the total voltage which could be measured across the TED leads. The Joule voltage is due to the resistance of the TED, and can be expressed using Ohm's law as

$$V_J = IR_j \qquad (11)$$

where R_j is the TED total electrical resistance. The Seebeck voltage is due to the temperature difference of the control and sink sides of the TED. The Seebeck Voltage is given by Equation (12):

$$V_\alpha = n(\alpha_p - \alpha_n)(T_s - T_c) \qquad (12)$$

Based on Equation (12), it can be seen that the Seebeck voltage generated by a given TED is a function of only the temperature difference. The voltage is independent of the current, and in fact the current can be zero (ex. disconnected and open circuit) and the Seebeck voltage would remain unchanged if control and sink temperatures are maintained. Putting all terms together, we arrive at Equation (13), which describes the voltage across the TED:

$$V_{TED} = IR_j + n(\alpha_p - \alpha_n)(T_s - T_c) \qquad (13)$$

2.3.2 Input Power Components

In the case where we are applying a current to the TED, all terms in Equation (13) can be multiplied by the applied current and we arrive at a relation describing the input power components to the TED. Sometimes the power delivered to the TED is known as the parasitic power, since heat generated in the TED is generally not a desired effect:

$$IV_{TED} = I^2 R_j + nI(\alpha_p - \alpha_n)(T_s - T_c) \qquad (14)$$

Equation (14) shows that the total input power to the TED is composed of a Joule heating component and a Seebeck component. The Seebeck component depends on the temperature difference between the control and sink sides of the

TED. This term accounts for the difference in heat absorbed and liberated at the control and sink sides of the TED, as driven by the Peltier effect (see Equations (2) and (3)). Note that, for a given current, the Joule heating component is always positive, and the Seebeck component can be either positive or negative, depending on the sign of ($T_s - T_c$) relative to the direction of current. For example, consider the scenario where the TED is operated in cooling mode (i.e. the direction of current is such that the control side absorbs heat and the sink side dissipates heat), however the heat flow from the boundary condition dictates that T_c must be higher than T_h. In this scenario, the Seebeck control-side temperature is higher than the sink-side temperature, for a positive current direction, thus the Seebeck term in the power equation is negative.

2.4 Characterization Methods

Many methods have been reported for the purpose of characterizing TED's, however most are based on the same concepts, and only a select few are widely used. The most popular metric by which to evaluate performance of a TED is the figure of merit ZT, defined in equation (8). Note again that this quantity is defined for a single material, and under limited assumptions can be extended to a TE couple. Despite this, the metric is commonly applied at the TE module level, often without knowledge on what the metric really implies for a TE module. To obtain the individual parameters needed for accurate performance prediction, the ZT figure of merit is not enough. Full characterization of a TED

is accomplished by resolving the following properties, listed below with their temperature dependencies:

- Module Seebeck Coefficent vs. TED temperature ($\alpha_{p,n} = f(T)$)
- Module Thermal Resistance vs. TED temperature ($R_{th} = f(T)$)
- Module Electrical Resistance vs. TED temperature ($R_J = f(T)$)

In the next sections, the most popular methods for characterizing TEDs will be reviewed and examined.

The Harman method for TED characterization was proposed in 1962, and has been a much utilized, much referenced approach [23]. The underlying methodology is based on the fact that under certain conditions, the figure of merit is related to the voltage components (see Equation (10)) across the TED. The relationship is given by Equation (15).

$$ZT = \frac{V_\alpha}{V_J} \qquad (15)$$

The main assumptions behind Equation (15) are that the input current and heat losses are small. This can be achieved using low input currents, typically on the order of 1/50th that of normal operating currents. A detailed list of assumptions can be found in [24].

Based on Equation (15), to measure the figure of merit for a TED at a temperature T, one only has to resolve the Seebeck (V_α) and Joulen (V_j) components of voltage across the TED. As we will see, the total voltage across the TED can be measured, and then, knowing either Joule or Seebeck Voltage component, the remaining (unknown) voltage component can be determine by

Equation (10). To resolve the voltage components across the TED, most of the methods in practice involve a scheme whereas a step-like current signal is applied to the TED, while the corresponding voltage measured. Since the resistive (Joule) component of the total TEC voltage is realized instantaneously, and the Seebeck component is a lagging effect and depends on the thermal time constant of the system, a high-speed data acquisition system (DAQ) can resolve these components. In illustration of the concept can be seen in Figure 5. The top graph in the figure represents the current applied to the TED, and the bottom graph in the figure represents the voltage observed across the TED at the same instant in time. As illustrated, only the Joule voltage component responds instantaneously with the current applied, while the Seebeck Voltage response lags. The lagging response of the Seebeck Voltage is due to the fact that this depends on the temperature difference across the TED (ΔT) and cannot be instantaneous. Since the Seebeck voltage is a thermal response, this depends on the thermal time constant of the system. To achieve a more robust measurement, often times a continuous input signal is applied, and measurements are obtained for a large number of on-off cycles. Polarity reversal is also performed to mitigate any effects of non-symmetrical boundary conditions on the TED, which would cause different results depending on input current polarity. Commercially available devices exist which operate on the Harman Method principle. One notable device produced by RMT Ltd [25] achieves a ZT measurement utilizing an applied AC current pulse (much like that in Figure 5,

only many times over), while measuring the components V_α and V_J at a steady state.

Since the Harman Method has been proposed, there have been many improvements proposed. A method known as the Transient method [19] is based on the same basic principal as the Harman Method, with the difference that instead of measuring points (I) and (II), point (II) and (Iii) are measured. Thus, instead of measuring the Joule Voltage, the Transient method proposes measurement of the Seeback voltage. The measurement can be repeated a prescribed number of iterations, and the results averaged for a robust measurement. It has been shown that the uncertainty in Z can be on the order of 10-25% however when applied correctly, and under most cases, the uncertainty is less than 5% [24].

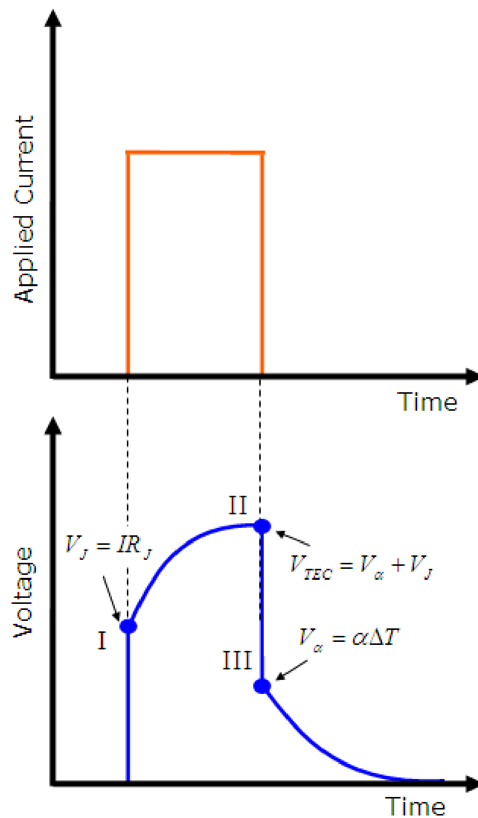

Figure 5-Applied current input and resulting output voltage on the TED based on the Harman Test Method.

The advantage in using the Transient method vs.the Harman Method, is that the ZT measurements can less sensitive to the TED time constant. Under conditions where the resonse of the TED is quite rapid (i.e. the TED having a relatively low time constant) measurement at location (I) can be difficult to obtain with high accuracy. The time constant of a typical TED thermo-element can be less that 1s. Thus, at a typical applied input current frequency of 40Hz, the Seebeck voltage can respond by as much as 5% [19]. Even though the Transient method is still somewhat subject to error under a small TED time

constants, it has been shown that by using extrapolation algorithms to identify the voltage at the precise time at which the current is switch off, a robust measurement of location (III) can be made [19]. Thus, the Transient method is one of the most popular methods used by manufacturers obtain the module ZT.

Furthermore, it has been shown that if the transient method is supplemented by additional measurements, the method can be used to determine the thermo-physical parameters needed to model TED performance. As was mentioned previously, these parameters include the Module Seebeck Coefficient, electrical resistance, and thermal resistance. The technique involves supplemental temperature measurement of the TED faces, as well as a fit of the data to a numerical model, assuming a set of thermal boundary conditions including convection, radiation, and conduction heat losses. A detailed description of the method can be found in [19]. Though promising results have been demonstrated using this methodology [19], the technique relies on highly controlled experimental conditions, and many assumptions with respect to the TED boundary conditions. As will be shown in later sections, direct measurement of heat flow into and out of the TED offers a conclusive empirical determination of boundary conditions. Moreover, the many challenges associated with device scaling under utilization of this procedure has not yet been addressed. In contrast, the developed metrology offers no limitations under device scaling, as well as many other clear advantages.

In another technique, The Transient is applied using a higher power and supplimented by not only face temperature measurements, but heat flow

measurements to obtain $\alpha_{p,n}$ R_j and R_{th} [26]. In the proposed method, it was shown the control and sink-side temperatures can be measured and used to compute the module Seebeck coefficient (MSC), per the following equation:

$$\alpha = \frac{V_\alpha}{T_s - T_c} \tag{16}$$

It is immediately evident that a large assumption is made using procedure to obtain the MSC. The assumption being made is that the measurements of the TED faces are approximately equal to the temperatures across the TE element faces. Device scaling can have drastic impacts when this assumption is present, since the interconnects and substrates can have relatively significant thermal resistance contributions as the device is made increasingly smaller.

Once the voltage components are resolved using the transient method, Equation (16) can be used with the source current to determine the electrical resistance of the TED. The heat flow from one side of the TED is estimated by placing a thermal mass on one side of the TED. Temperature rise vs. time in the thermal mass can be related to the heat flow into the mass, and by also measuring the control and sink-side temperatures, the following equation can be used to compute the thermal conductance of the TED:

$$K = \frac{\alpha I T_h + \frac{1}{2} I^2 R - Q_s}{T_s - T_c} \tag{17}$$

Again, the major issue with this method is that the accuracy relies on the assumption that element-level behavior is the same as module-level behavior. Equation (17) is based on the earlier Equation (9), which is derived using an

energy balance at the TE element level. A main assumption in the derivation of this equation is that the TE interconnects and substrates are ignored [15].

Once the Seebeck Coefficient, electrical resistance, and thermal conductance are known, the method employs Equation (18) to compute the figure of merit Z.

$$Z = \frac{\alpha^2}{RK} \tag{18}$$

Figure 6 summarizes the main assumption behind this method. Almost all the equations offered ignore contributions from the interconnects and substrates. As mentioned, these assumptions can have drastic consequences for even relatively large TEDs. An explanation on how the measured face temperatures are extrapolated to the TE elements is not offered in the paper. A similar approach is performed in [27] with a slightly modified test configuration.

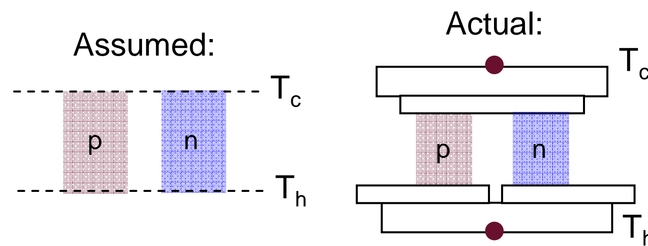

Figure 6-Assumed vs. actual configurations under the TED test methods proposed in [26] and [27]. The assumptions can lead to significant error under device scaling towards smaller TEDs.

Another Novel approach to measure ZT was proposed in [28]. In this method, a heatflow is assumed across the TED, and the temperature difference

(ΔT) is measured in two configurations: open circuit, and closed circuit. A relation is derived, whereas ZT dimensionless figure of merit can be computed using the ratios of the two ΔT's obtained. The advantage in this measurement is that measurement electronics are simple, since all measurement can happen at a steady-state, and furthermore, adiabatic assumptions present in the Harman approach do not apply. The formula derived in the paper to determine ZT is the following:

$$\frac{\Delta T_{open}}{\Delta T_{closed}} = 1 + ZT \tag{19}$$

Where ΔT_{open} and ΔT_{closed} are the temperature differences across the TED in an open-circuit and closed circuit configurations, respectively. The derivation of Equation (19) is very strait-forward.

Many creative methods have been proposed to measure the parameters needed to characterize TED's. Despite having shown great results, none of the proposed methods provides a way to empirically quantify the heat-flow into and out of the TED. An accurate heat-flow measurement is not only critical to estimate TED thermal resistance, but it allows extrapolation of the temperature difference measured across the TED faces to that which exists across the TED elements. It will be shown that measurement of the heat-flow is not only a valuable, but critical to deriving parameters for accurate modeling. The advantage is especially prominent under aggressive device scaling, as has been the trend in recent years.

2.5 Modeling Methods

Because of the complexity and number of variables involved, full understanding of TED and TED system performance requires some form of modeling. Consider that the heat flow on the control and sink side of the TED depend on the local temperature. Since the heat flow effects the temperatures, and temperatures effect the heat flow, an iterative solution is required to solve for steady-state system temperatures when a TED is present. In addition, if temperature dependant properties are considered, these properties must be evaluated iteratively. The choice of modeling method depends mostly on how much detail is required from the output. If the problem can be considered one-dimensional (1D), that is, temperature and boundary conditions only are assumed to vary in one spatial domain, then the modeling can be greatly simplified. Conversely, if variation in all spatial domains is relevant, then the general three-dimensional (3D) form of the heat diffusion equation must be assumed, and the PDE must be solved for each unit in the 3D spatial domain. For example, if a TED is used to cool a CPU which has a spatially-varying power, a 3D solution would be desirable, to capture the heat spreading effects present in the problem, and how this effects die temperatures. Fortunately, TED systems lend themselves well to the 1D assumption, since the heat-flow occurs dominantly in only one direction. Because of this fact, temperature gradients are typically much larger in the direction normal to the TED, as opposed to in-plane temperature gradients, which, in most cases can be safely neglected. Supporting experimental data will be shown in a later section.

One of the most common forms of TED modeling is through the use of thermal-electrical analogies. If the primary heat paths can be identified, each of these can be modeled as a conductor in an electrical circuit. As in electrical circuits, under these modeling assumptions, current (i.e. heatflow) can only reach a point in the circuit through discrete paths. Also, the models can be easily extended to transient analysis through the electrical capacitance, but used to represent a thermal capacitance. In the thermal-electrical analogy, there is no such thing as inductance, since there is no equivalent to a magnetic field in the thermal domain. Consequently, all electrical network diagrams representing thermal systems are composed of circuits with only resistive (or conductive) and capacitive components.

When modeling a thermal system via an electrical network, two primary forms have been proposed, namely, the Foster network and the Cauer Network approaches [29, 30]. The two types of networks can be seen in Figure 7. In the figure, the thermal resistances are represented as blocks with R_1, R_2, etc, and the thermal capacitances are represented as capacitance nodes with capacitance C_1, C_2, etc. The capacitances are volumetric heat capacitances, since each body is considered a storage medium, with the total volume of the object representing the storage domain.

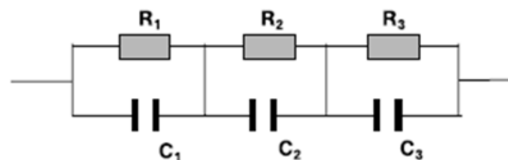

a) Foster Network

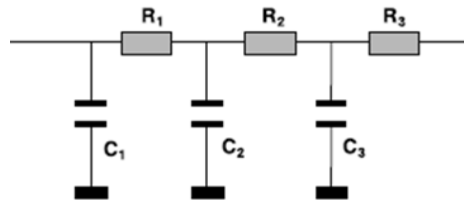

b) Cauer Network

Figure 7-Foster vs. Cauer network configurations[30].

Almost any thermal system where discrete heat paths can be assumed, can modeled with either approach, as there is always a way to interchange a Cauer Network with a Foster Network. Despite this, there are distinct differences in the two approaches. The primary difference is that the Cauer network capacitances and resistances are physically meaningful, whereas in the Foster network approach, the parameters are not physically meaningful. This is the case since, in the classical understanding of thermal transport, the movement of heat does not correspond to movement of any type of particle, only the storage of energy in the atoms comprising the object's mass. Because the Foster network considers only thermal capacitances as referenced to ground (ie some reference or baseline energy storage state), this approach represents the thermal system in a more physically-meaningful way. The RC network approach has been shown to be in good agreement with finite element numerical solutions when applied to situations which can be considered 1D [29].

The Cauer network modeling approach, as applied to TED's has been investigated, and found to offer accurate results. In a study done on a

thermoelectric refrigerator, output form a developed Cauer model was compared the model to experiment varied by +/- 7% across a large span of operating conditions [31]. A nice advantage in using the Cauer network approach is that a high amount of details of the TED can be included in the model. For example, the Cauer network approach was used to model and evaluate the effects of electrical contact resistance, as well as substrate thermal conductivity in an on-chip peltier cooler [32]. It has also been shown that the TED power supply could be easily included in the model, and moreover, that by including a non-ideal power supply and feedback voltage from the TED, the model was much better at representing the system from an energetically correct standpoint [32].

Finite-element methods are also widely used to characterize TED systems. Companies like ANSYS offer very powerful software tools which allow the ability to easly include TED's in a system model. ANSYS-Icepak numerical modeling software includes macros which can be easily inserted into any model. A tutorial is available for download on the Marlow Industries website which explains how TED macros can be included in a model and automatically contain information on a specific, off-the-shelf TED model [33]. This offers a nice convenience to the designer, as prospective TED designs can be modeled for system performance before they are purchased. In cases where a custom TED must be evaluated, it is a relatively easy task to build and model a TED from scratch. Many of the leading numerical software packages allow temperature-dependant heat sources, which can be used to generate the temperature-dependant control and sink-side heat flux. Good match with experimental data has been show for macro-scale

TEDs [34], as well as micro-scale TED's [8]. In both of the studies referenced, volume-average properties were used to model the thermoelectric elements, and both studies included details such as electrical contact resistances between the electrical interconnects and the thermo-elements.

3. EMPIRICAL CHARACTERIZATION

3.1 Metrology Overview

As was discussed in the previous section, modeling allows the designer to understand and optimize the critical parameters which influence the performance of a TED system. For accurate prediction, it is critical that the input parameters are accurate, and applicable to the temperature range of interest. It is only from direct measurement these critical parameters can be obtained. The measurement method we will propose offers the high measurement confidence needed to make accurate performance predictions. Moreover, due to the fundamental simplicity of the method, results do not depend on any heat flow or temperature assumptions, as these are directly measured for both control and sink-sides of the TED. In this test method, a TED can be analyzed in a state which closely represents the use-condition (i.e. the TED is subject to a heat load, under a given current and voltage input). All temperatures and heat flows can be directly measured. Due to the in-situ nature of the method, the metrology use can easily be extended to many other fundamental characterization studies, including reliability studies, and control scheme studies. The metrology, as will

be show, offers many unique capabilities not available using other characterization methods.

A schematic of the metrology can be seen in Figure 8 and Figure 9. The metrology system consists of primarily two large aluminum blocks which can be actuated together with a given pressure, and between which a TED can be inserted. The blocks are the same footprint area as the TED being studied, and serve as a 1D conduction heat-flow path through which heat flow can be directly measured. Insulation was added to the periphery of the aluminum blocks to minimize the heat loss from the sides. To measure the heat flow through the aluminum blocks, a temperature gradient is measured normal to the TED faces, using thermocouples embedded at known locations – these measurement locations are represented in the figure as T_1, T_2, and T_3 for the lower aluminum block, and T_4, T_5, and T_6 for the upper aluminum block. Below the lower aluminum block, a heater is used to simulate power generated from a device. Insulation was included under the heater to minimize heat loss from the bottom of the setup, even though the actual power through the TED is measured directly using the thermocouples. Above the top aluminum block, a liquid-cooled cold plate is used as a heat sink. A thermal interface material (TIM) is used between the TEC and aluminum block faces to ensure adequate thermal contact.

All physical temperature measurement locations cam be seen in Figure 8. In the metrology, thermocouples are present across the top and bottom faces of the TED. The TED face temperature is measured in three in-plane locations on each the top and the bottom of the TED.

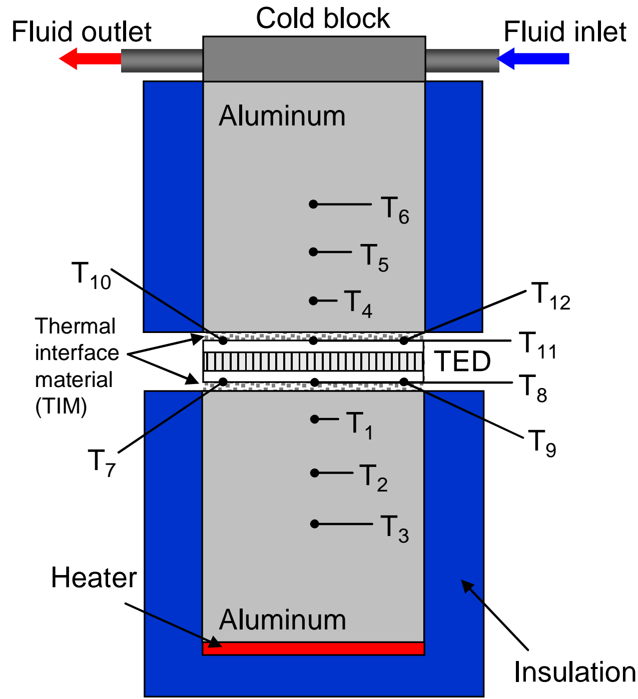

Figure 8-TED metrology schematic with thermocouple locations.

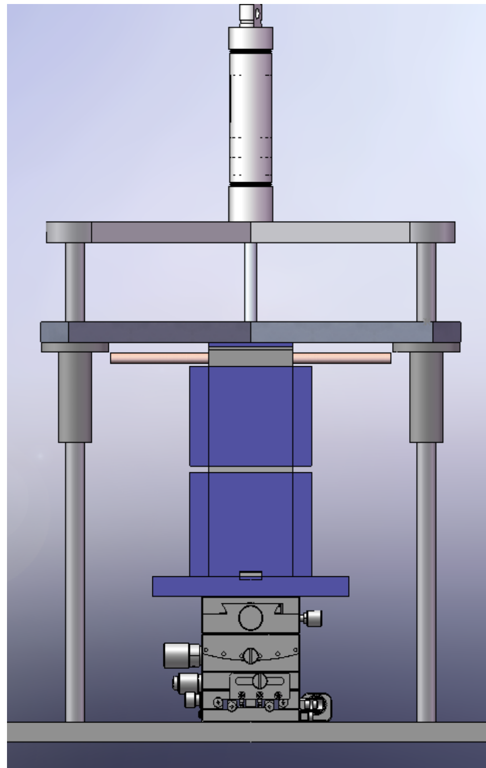

Figure 9-TED Metrology Schematic

The off-center locations measure diagonal corners of the TED; these measurement locations are included to allow the ability to quantify the temperature gradient across the TED face. Thermocouples at locations T_8 and T_{11} measure the temperatures at the center lower and upper TED faces, respectively. Thermocouples at locations T_7 and T_9 measure diagonal corners on the top of the TED, and T_{10} and T_{12} measure diagonal corners on the bottom. Inputs and outputs are listed in detail in Tables 2 and 3, respectively. For the most part, inputs allow the user to change the operating temperatures, as well as to control the TED functionality by changing the supplied current. Outputs are direct measurements (T_1-T_{12}, Q_c, Q_s) as well as derived quantities (R_j, R_{th}, and $\alpha_{p,n}$), which will further be explained in detail. Figure 9 shows a schematic drawing of the measurement fixture.

Table 2-Metrology inputs and effected quantities.

No.	**Metrology Inputs**	**Resulting Effect (due to a change in the input)**	**Effected Quantity**
1	Heater Power	Operating temperature	T_1-T_{12}
2	Chiller temperature	Operating temperatures	T_1-T_{12}
3	TED current	Heatflow and operating temperatures	Q_s, Q_c, T_1-T_{12}
4	Actuation force	TIM resistance (or conductance) at top/bottom TED faces	R_1 (or K_1)

Table 3-Metrology outputs and associated quantities.

No.	Metrology Outputs (directly measured or computed from measured)	Symbol
1	Heatflow no the sink or control side of the TED	Q_s, Q_c
2	System and TED temperatures	T_1-T_{12}
3	TED power	P
4	TED electrical resistance	R_J
5	TED thermal resistance	R_{th}
6	TED Seebeck Coefficient	α_{p-n}

3.2 Accuracy Evaluation

As a first step after building the measurement setup, experiments were performed for the purpose of establishing confidence in the output. It was determined that the best way to check the accuracy of the metrology was to measure the thermal resistance of a known material (in place of a TED), and check that this number was close to that computed from the thickness and known conductivity of the sample. A 40mm x 40mm x 3mm solid copper block approximately the same geometry as a TED was used for this evaluation. To measure the thermal resistance of a given sample, the heatflow through the sample, and temperature gradient across the sample must be measured. After some initial runs to determine what settings would yield temperatures in the range of interest, the test parameters were chosen to be:

- Simulated device power (heater) = 100W
- Chiller temperature = 288.15 K
- Actuation pressure = 40psi
- TED current: NA, no TED used for the accuracy evaluation. A 40mm x 40mm x 3mm Cu block used as a mock TED.

It was determined that a test time of 30 minutes resulted in steady-state temperatures. Results from the test can be seen in Figure 10, where all steady-state temperatures are plotted vs. location measured.

Heat-flow is measured using the thermocouples embedded in the Aluminum blocks. Knowing the temperature gradient, the distance between each thermocouple, and the conductivity of the aluminum, the array of thermocouples in the aluminum blocks can be used to calculate the heat flow. The conductivity of aluminum is assumed to be 167 W/m-K [35]. The measured temperature gradient for both the top and bottom blocks can be seen in Figure 11. The distances denoted in the plot are with reference to the interface of the aluminum block and the thermal interface material. The upward direction from the interface is denoted as positive, while the downward direction denoted as negative.

As shown in Figure 11, the top block temperatures are lower than the bottom block temperatures. This is due to the fact that the lower block is closer to the heater. As is also shown in Figure 11, a linear regression of temperature versus length gives an R^2 of 1.000. This shows that over the length where the heat flow is measured, very little heat is lost through the sides of the metrology.

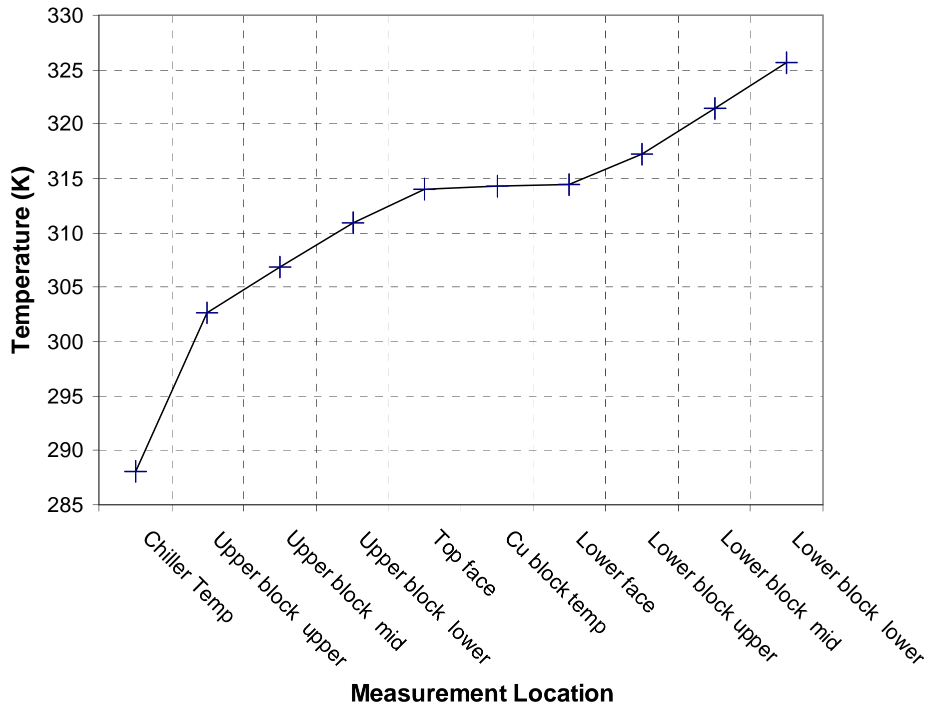

Figure 10-Temperatures as measured at various locations for the metrology accuracy study.

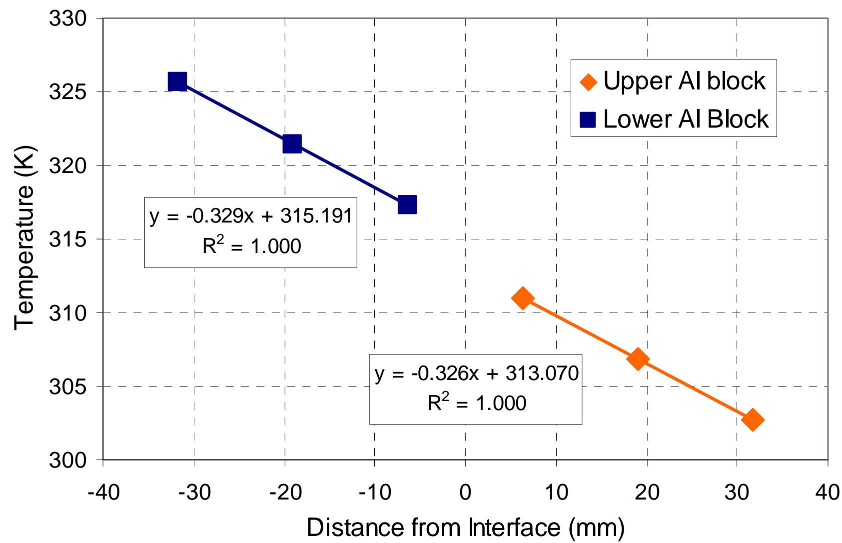

Figure 11-Temperatures as measured at various distances in the Al blocks. Slope of the temperatures vs. distance is use to calculate the heat-flow.

The slope of the line can be used in Fourier's law to determine the heat-flow, as shown in Equation (20).

$$Q = -k_{al} A \frac{dT}{dx} \tag{20}$$

where k_{al} is the conductivity of Aluminum, A is the area, and dT/dx is the slope in temperature vs. length along the aluminum block. If an average of the two slopes is used to compute dT/dx, a power of 87W heat-flow through the sample. This indicates that around 13% of heat is being dissipated through the bottom and sides of the setup.

Using the thermocouples on either side of the copper block, the ΔT across the sample faces is measured to be around 0.34℃. The measured thermal resistance should be equal to that which we expect from the material, knowing its thickness, thermal conductivity, and area. Equation (21) gives the expected relationship:

$$\frac{\Delta T}{k_{al} A \frac{dT}{dx}} = \frac{l}{k_{cu} A} \tag{21}$$

where l is the thickness of the copper sample, k_{cu} the conductivity of the copper sample, and ΔT the temperature difference across the copper sample. Note that area of the sample is the same as the area of the aluminum block used to measure the heat-flow. After re-arranging terms and canceling area, the result is Equation (22), which represents the expected temperature difference across the copper sample.

$$\Delta T = \frac{l \cdot k_{al}}{k_{cu}} \frac{dT}{dx} \tag{22}$$

Assuming 401 W/m-K as the conductivity of copper [36], an expected temperature difference of 0.41 K across the copper sample is computed. Since a temperature difference of 0.34K is measured, the error in temperature difference is less than 0.1K. Since thermocouples are being used for the measurement, this error is more than acceptable, since quoted accuracy of most thermocouples are +/- 0.5℃ or greater[37]. Table 4 shows the measured temperatures at steady-state. Note the great agreement between the sensors on the faces of the aluminum blocks; all face temperatures agree to within 0.11℃. The good agre ement between face thermocouples indicates that that there is good contact between the thermocouple and the TED face. Table 5 shows a summary of the computed heat-flow through the upper and lower blocks. As indicated in the table, both upper and lower aluminum blocks have the same thermal conductivity and cross-sectional area.

Table 4-Temperatures measured in the accuracy study.

Thermocouple Number	Location	Steady-State Temperature (K)
1	Lower block upper	317.49
2	Lower block middle	321.65
3	Lower block lower	325.83
4	Upper block lower	310.96
5	Upper block middle	306.81
6	Upper block upper	302.69
7	Lower block face corner 1	314.43
8	Lower block face center	314.48
9	Lower block face corner 2	314.54
10	Upper block face corner 1	314.06
11	Upper block face center	314.14
12	Upper block face corner 2	314.16

Table 5-Summary of Heat flow calculations from the accuracy study.

Upper/Lower Al block	Quantity	Units	Value
Upper	Thermal Conductivity	$Wm^{-1}K^{-1}$	167
Upper	Area	mm^2	1600
Upper	Slope (dT/dx)	Kmm^{-1}	-0.329
Upper	R squared	No units	1.000
Upper	Heatflow	W	87.01
Lower	Thermal Conductivity	$Wm^{-1}K^{-1}$	167
Lower	Area	mm^2	1600
Lower	Slope (dT/dx)	Kmm^{-1}	-0.326
Lower	R squared	No units	1.000
Lower	Heatflow	W	87.74

3.3 Extrapolation Face Temperatures

One of the most prominent benefits of the proposed metrology is that it allows the ability to evaluate TED internal temperatures. Since there is no other known method to experimentally determine TED internal temperatures, this methodology adds great value to the field of TED characterization. Extrapolation is used to determine the thermal resistance and MSC. The method used to extrapolate from

face temperatures will be explained here in detail before showing the measurement procedure and results.

Since measurements are performed at the Alumina faces of the TED and not directly across the TE elements, an extrapolation must be performed to arrive at temperatures at these locations. Figure 12 shows a summary of the temperature locations of interest. Measurements are acquired at T_8 and T_{11}, and temperatures at T_c and T_s are desired. To simplify the analysis, each layer is being treated as a homogeneous layer. It can be seen from the figure that in order to determine the temperatures T_s and T_c, the thermal resistances of the alumina substrates and interconnects, as well as the heat flow must be known. A very thorough analysis may include a teardown of the TED in question to determine exactly what materials and thicknesses are present. This would be especially important if the thermal resistance of the interconnects and substrates were comparable in value to that of the TE elements. This is often the case for very thin TED's. For this device an estimation will suffice, since the TE element layer thermal resistance is likely large relative to the interconnects and substrates. For this analysis, the thermal resistances will be estimated by assuming they are made of commonly used materials.

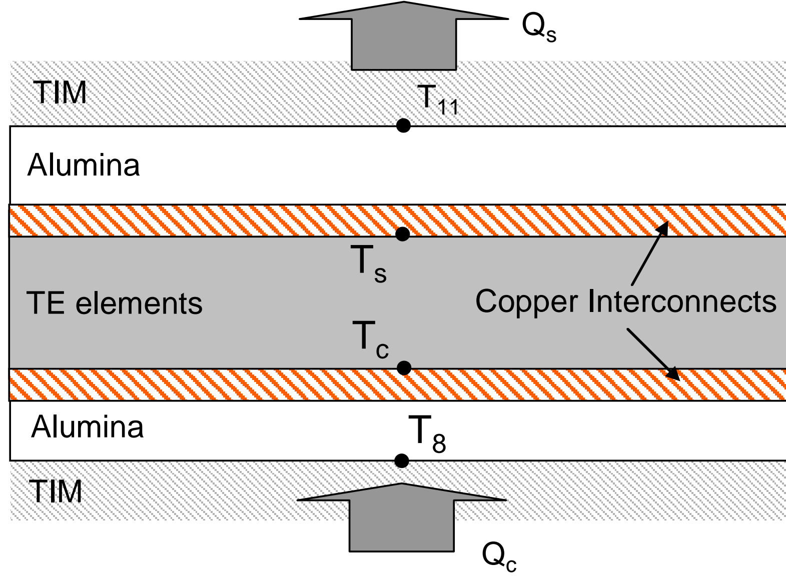

Figure 12-TED thermal resistance stack-up.

To compute the temperatures at the TE faces, Equation (23) through Equation (26) show the calculations.

$$R_{si} = \frac{l_{alo2}}{k_{alo2}A} + \frac{l_i}{k_i A} \quad (23)$$

$$T_c = T_8 - Q_c R_{si} \quad (24)$$

$$T_s = T_{11} + Q_s R_{si} \quad (25)$$

$$\Delta T = T_s - T_c = T_{11} - T_8 + R_{si}(Q_s + Q_c) \quad (26)$$

where R_{si} is the effective thermal resistance of the substrate and interconnect layers, k_{alo2} and k_i the substrate and interconnect thermal conductivities, respectively, l_{alo2} and l_i the thicknesses of the alumina and interconnect layers, respectively. The thermal conductivity of the alumina can be found in literature to be 36 $Wm^{-1}K^{-1}$ [38], and the thickness of this layer can be directly measured to be 0.75mm. As for the

interconnects, typically these are made from a material which is a good electrical and thermal conductor, so it will be assumed that these are made from Copper. The conductivity of copper can be found to be 401 $Wm^{-1}K^{-1}$[36]. Finally, if we assume that the fraction of area which the interconnects comprise is around 30% of the total TED area, and furthermore that the thickness of the interconnect is 200µm, we can compute the thermal resistance R_{si}. A summary of the computed thermal resistances can be seen in Table 6. As shown in the table, the alumina thermal resistance is around 0.013KW^{-1}, and the interconnect thermal resistance is around 0.001KW^{-1}. As will be shown, for this TED, these layers represent around 2% of the total thermal resistance of the TED. The amount is not substantial for this particular TED, however the contribution from these layers should not, in general, be ignored since the error can be quite large in cases where the overall thickness of the TED is smaller.

Table 6-Summary of thermal resistances of substrate and interconnect layers.

	Units	**Alumina Substrate**	**Cu Interconnects**
Thickness	m	7.50E-04	2.00E-04
Thermal conductivity	$Wm^{-1}K^{-1}$	36	401
Area Fraction	--	1	0.3
Effective A	m^2	0.0016	0.00048
Effective R (single layer)	KW^{-1}	0.013	0.001

3.4 TED Measurement Results

Now that the metrology output has been validated, the system can be used with confidence to measure a TED. As was mentioned earlier, there are three parameters which must be captured to fully model or describe a TED's performance in any system:

- Module Seebeck Coefficent vs. TED temperature ($\alpha_{p,n} = f(T)$)
- Module Thermal Resistance vs. TED temperature ($R_{th} = f(T)$)
- Module Electrical Resistance vs. TED temperature ($R_j = f(T)$)

To demonstrate measurements on the metrology, a TED purchased from Kryotherm has been evaluated. The TED selected for measurement is the Kryotherm model "Drift-0.8". Specifications can be found at the Kryotherm website [13].

3.4.1 Thermal Resistance Measurement

The thermal resistance of the TED is the easiest parameter to measure of the three required. TED thermal resistance is given by Equation (27):

$$R_{th} = \frac{\Delta T}{Q} \tag{27}$$

Where ΔT is the temperature difference extrapolated to the TE elements, and Q is the average heat flow as measured using the top and bottom aluminum blocks. The measurements can be acquired using the thermocouples embedded in the aluminum blocks and at the faces (contacting the TED). For this test, the TED is inactive (i.e. no current is applied), as we do not want generated power altering the measured temperatures. Measurements can be obtained at various temperatures by leaving the chiller temperature constant and varying the input power to the heater. Figure 12

shows the thermal resistance as measured as the power to the heater is varied 25W to 125W at increments of 25W (5 points total). By varying the power in such a way, we are able to impose TED temperatures from 300K to around 350K, covering a large span of the operating temperature range of the TED. Since the TED is not generating power, the temperature of the geometric middle of the TED is simply the average of the face temperatures. It can be seen from figure that the thermal resistance varies from about 0.65 K/W to about 0.705 K/W, or around 8%, over the temperature range of interest. The thermal resistance is simple but crucial piece of data in describing the performance of a TED. To capture the behavior in the temperature domain of interest, we perform a least-squares fit using a polynomial. As will be demonstrated, this allows an easy implementation of the TED thermal resistance into a model.

3.4.2 Module Seebeck Coefficient Measurement

The Module Seebeck Coefficient (MSC) is dependant on the number of couples in the TED, and the individual Seebeck coefficients of the p-type and n-type thermo-elements. The MSC is defined in Equation (28):

$$\alpha_{p,n} = n(\alpha_p - \alpha_n) \tag{28}$$

where $\alpha_{p,n}$ represents the MSC.

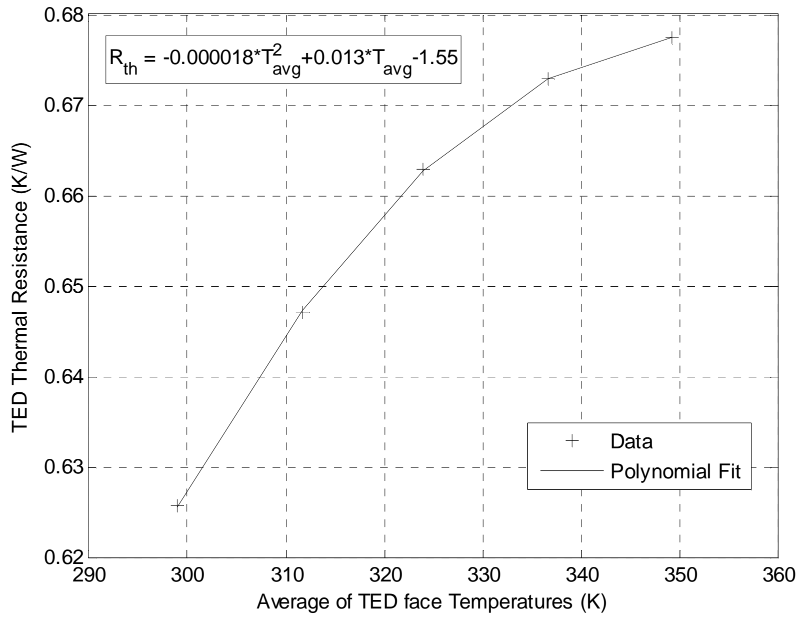

Figure 13-TED electrical resistance vs. temperature as measured in the TED Metrology.

The MSC can be determined if the temperature difference across the TE elements is known, as well as the open-circuit voltage which the TED generates. Expressed on a per-element basis, the MSC can be computed using equation (29).

$$\alpha_{p,n} = \frac{V_\alpha}{2n\Delta T} \tag{29}$$

In the particular TED we are studying, there are 200 thermocouples.

Like the thermal resistance, the MSC is a function of temperature. To capture the temperature dependence, the same procedure can be employed as was performed for the thermal resistance, i.e. the chiller temperature is held constant and the power to the heater is varied. The results of the test can be seen in Figure 14. As shown in the figure, the parameter has a small temperature dependence. As with the

thermal resistance, a least-squares fit using a polynomial is employed to capture the functional relationship with temperature. Because the measurement of the MSC requires the same test parameters as the thermal resistance measurement, this data can be acquired simultaneous to that of the TED thermal resistance. By performing the tests simultaneously this allows reduction in the total test time.

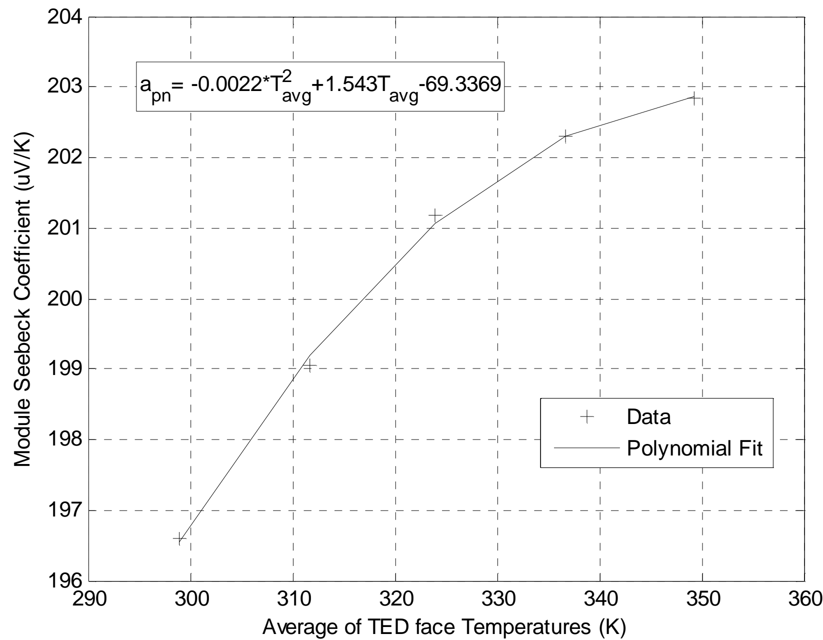

Figure 14-Module Seebeck Coefficient vs. temperature as measured in the TED metrology.

Though the exact composition of the thermoelectric material in this particular TED is proprietary to the manufacturer, the resutlts can be compared to data from what is likely to be the TE material of choice. The manufacturer website for the evaluated TED states that the TE material is “traditionally made of Bismuth Telluride-based alloy[s]” [39]. Based on published data, the Seebeck Coefficient of Bismuth

Telluride solid solutions can range from 116 to 227 μVK^{-1} for p-type semiconductors and -115 to -247 μVK^{-1} for n-type semiconductors [40]. Direct measurement on high performance n-type and p-type Bismuth Telluride alloys showed values of -227 μVK^{-1} and 221 μVK^{-1}, respectively[1] [41]. The MSC for this TED is measured to be around 200μVK^{-1}, so if the TE material is a Bismuth Telluride alloy, the measurement results are in the range of expected values.

3.4.3 Electrical Resistance Measurement

The TED electrical resistance dictates the amount of Joule heating generated by the TED in an active state. As can be seen from Equation (10) the voltage across an active TED is a sum of the Seebeck Voltage and the Joule Voltage.

$$V_{TED} = V_J + V_\alpha \qquad (10)$$

As was mentioned previously, the Seebeck voltage component is a function of the Seebeck coefficient and the temperature difference across the TED. The Joule voltage is a function of the current through the TED and the electrical resistance of the TED. The Joule voltage cannot be directly measured, since a measured voltage across the TED in an active state would have both Joule and Seebeck voltage components. However, since the MSC is known, a measurement of the extrapolated ΔT can be used to determine the Seebeck voltage, and this quantity can be used in Equation (10) with the measured TED voltage in an active state, to determine the joule voltage. Once the joule voltage is determined, the TED electrical resistance can be computed by dividing the Joule voltage by the current. Equation (30) shows the

[1] Measurements were performed at 298K on as-grown alloys.

calculation which must be performed to compute the TED electrical resistance. Not that all quantities on the right hand side are known from the measurement.

$$R_j = \frac{V_{TED} - \alpha_{p,n} \Delta T}{I} \quad (30)$$

To capture the full range of operation, data was collected at current levels of 2A, 4A, 6A, and 8A applied to the TED. For each test, all metrology temperature and voltage data was measured. The following figure shows the computed TED electrical resistance, as a function of the average of the TED face temperatures. The resulting resistance values for each apply current level is displayed in Figure 15. Resistance values were observed to scale linearly with $T_{avg.}$ A least-squares fit was performed and can be seen in Figure 15. The error in the linear regression resulted in an R^2 of 0.986, indicating that the corresponding functional relationship can accurately describe the TED electrical resistance with temperature, for multiple current levels.

In this case, it is important to note that T_{avg}, (the arithmetic average of the measured TED face temperatures) may not be equal to the true average temperature, since the TED is undergoing internal Joule heating. Power generation in the TED causes the temperature distribution through the TED to be non-linear. Since the measured TED electrical resistance is captured for many different current levels, and has low error about the linear fit, it can be assumed that the average of the TED face temperatures varies very little from the true average and can be used as a correlation parameter to establish the temperature dependant nature of the electrical resistance.

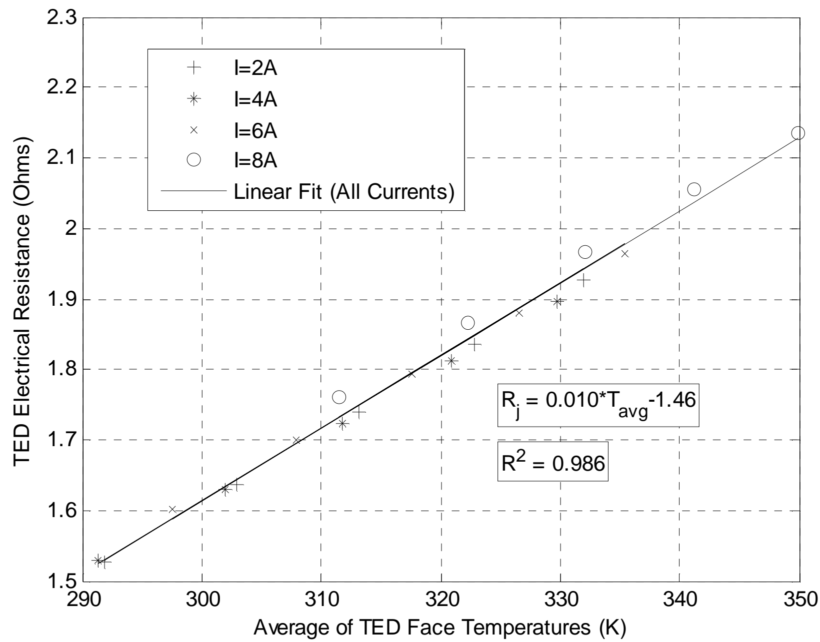

Figure 15-TED Electrical Resistance vs. temperature as extracted from passive and active TED measurements.

Published data for this particular TED states an electrical resistance of 1.65 Ohms at a temperature of 298K, with a tolerance of ± 10% [13]. Per figure 15, the measurement data shows an electrical resistance of about 1.6 Ohms at 298K. Thus, the measured data is in great agreement with manufacturer measurements.

3.5 Empirical Validation of Measured Parameters

Accurate TED performance prediction is largely determined by the ability to predict the amount of waste heat which TED generates (i.e. the parasitic power). As discussed previously, the parasitic heat loss manifests itself in two separate components: Joule heating, and Peltier heating. The components can be seen in the terms in Equation (14).

$$IV_{TED} = I^2 R_j + nI\alpha_{p,n}\Delta T \tag{14}$$

Note that the parasitic heat loss depends on two parameters which have been measured. The parameters in their functional forms, as determined in the previous sections are shown in equiatons (31) through equations (33).

$$R_J = (0.01T_{avg} - 1.46)\ \Omega \tag{31}$$

$$\alpha_{p,n} = (-2.2 \times 10^{-3} T_{avg}^2 + 1.54T_{avg} - 69.34)\ \mu VK^{-1} \tag{32}$$

$$T_{avg} = \frac{T_8 + T_{11}}{2} \tag{33}$$

The metrology offers the unique ability to check the measured parameters (Equation (31) and Equation (32)) by comparing the power computed using equation (14) and the difference between the heat flow measured on the sink and control sides of the TED (in an active state). Figure 16 shows the correlation of predicted vs. measured parasitic power for the data set which was used to generate the parameters. Figure 17 shows the same correlation, but for a completely different set of input currents, namely I = 1, 3, 5, 7, and 9A. It is clear that the measured parameters do a great job predicting the parasitic heat loss from the TED.

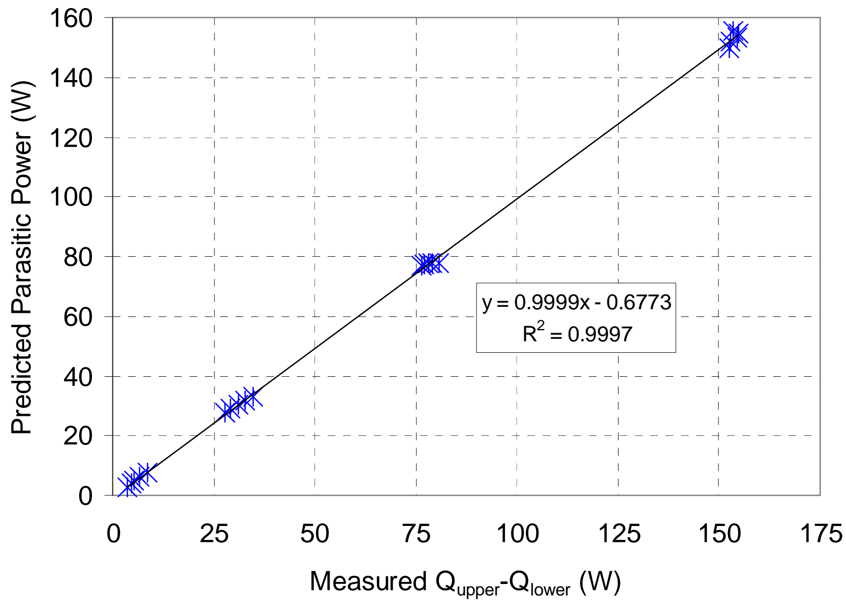

Figure 16-Correlation between measured power and computed power for experiments used to generate parameters.

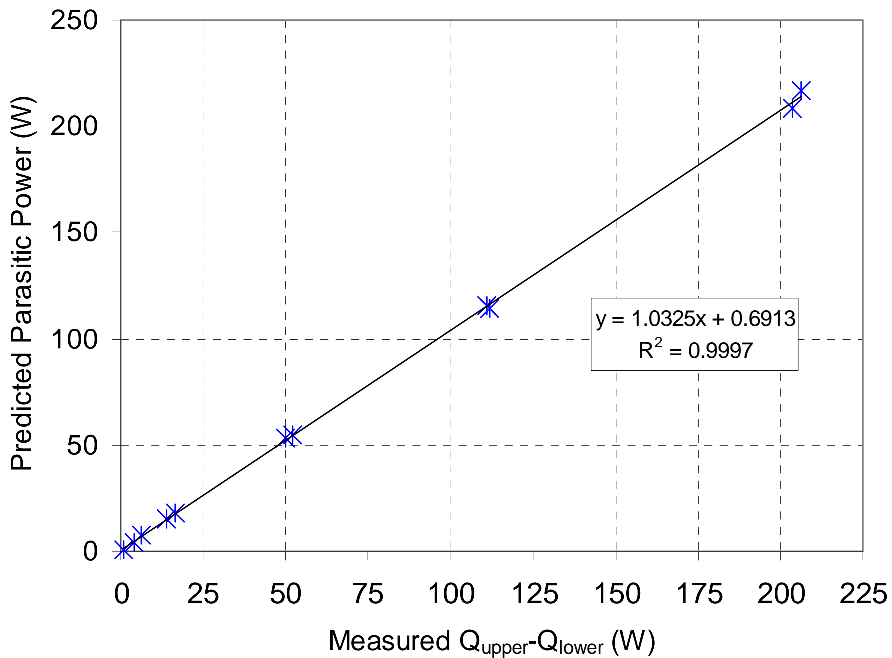

Figure 17-Correlation between measured power and computed power for an independent set of current levels: I = 1,3,5,7, and 9A.

4. MODELING

4.1 Model Overview

One of the main goals in deriving TED parameters from experiment is so the parameters can be used in a model to predict performance of a TED in a system. A model of the metrology system will be shown, to offer support that the parameters we have derived from metrology can indeed allow us to predict the TED performance. A model of the TED metrology system will be presented, and it will be shown that the temperatures can be predicted using the derived TED parameters.

Since the TED Metrology is a simple 1D system, it will be modeled using a resistive network. This approach is ideal for systems where heat paths are clearly defined. Resistive networks are relatively simple to program, and the employed resistances are physically meaningful. Since steady-state performance is of interest, any capacitances in the system can be treated as open connections. Thus, for this analysis, it does not matter if either the Cauer Network or Foster Network modeling approaches are selected, since both schemes would reduce to the same purely resistive network under steady-state conditions.

Consider a metrology system where the TED comprises a sub-system. Since the TED itself is them most complicate part of the system, we will describe the TED sub model separately. A physical representation can be seen in Figure 18, where the thermal resistances can be seen overlaid with a picture of the metrology system. Heat can be generated from either the heat source on the bottom of the metrology (Q_{in}) or the TED subsystem (from parasitic TED losses). This heat from these sources can travel to any one of the temperature boundary conditions, represented by

$T_{chiller}$ or T_{amb}. Heat which moves to the T_{amb} locations represents that which escapes the system via convective heat loss on the sides of the metrology. Though this is somewhat prevented by the insulation layer surrounding the aluminum blocks, it represents a sizable fraction of the energy input to the system via the bottom heater (supplying Q_{in}), and must be taken into account. The physical locations of the temperatures of interest in the model can also be seen in Figure 18. Theses locations directly correspond to locations in the experiment setup, and nomenclature is consistent (see Figure 8). As can be seen in Figure 18, there are four locations internal to the system which are of interest (locations 6, 11, 8, and 3). The temperatures at these locations will be outputs from the model, and can be directly compared to data output from the experiment. T_{amb} and $T_{chiller}$ represent boundary conditions to the model – these will be obtained from experiment, and input to the model. Most of the resistances in Figure 18 can be obtained from experimental data generated from the metrology. The conductances $K_{loss,top}$ and $K_{loss,bot}$ each comprise conduction and convention thermal conductance, and are not trivial to analytically determine. The quantities used for these conductances are those which give the best match with experimental data at baseline conditions (i.e. no TED power case with various Q_{in}). This will be discussed in more detail in the next section.

Figure 19 shows the resistance network model representing the metrology with the TED sub-system.

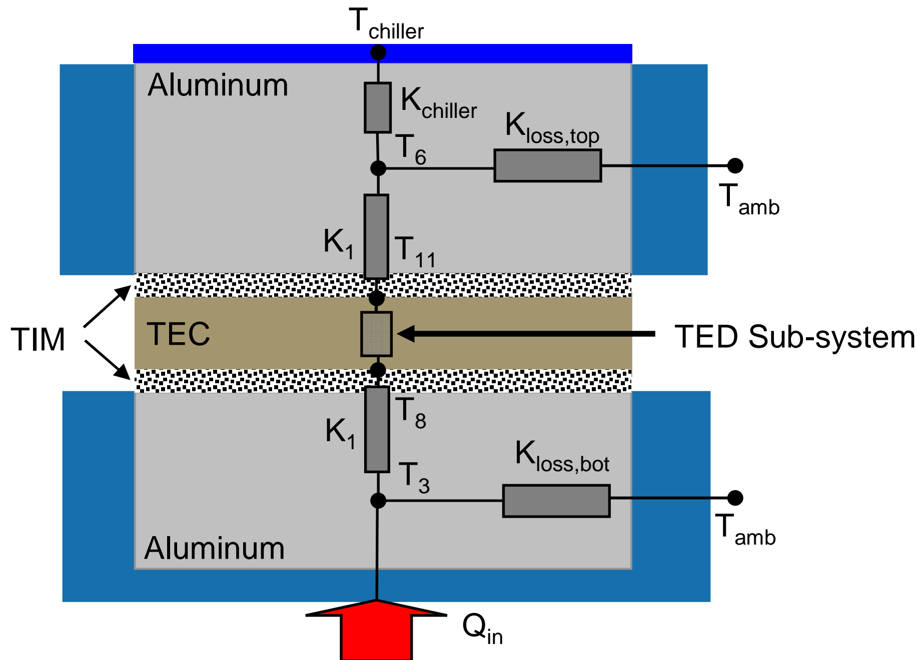

Figure 18-Schematic of the steady-state system-level metrology thermal model, overlaid with the physical system.

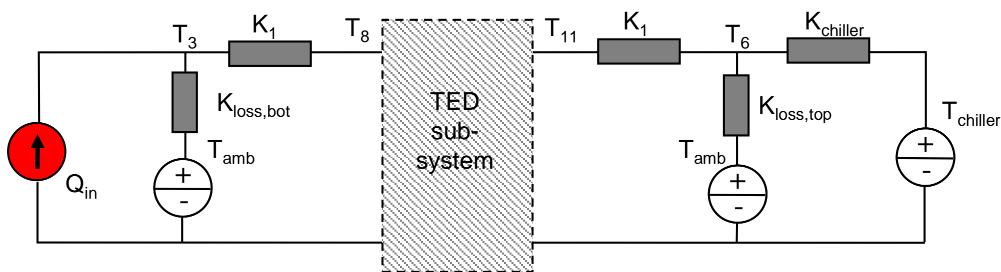

Figure 19-Electrical network schematic of the metrology system-level thermal model.

As shown in Figure 19, the thermal aspects of the system are represented using an electrical analogy. In the system, rectangular blocks represent thermal conductances, voltages sources represent temperature boundary conditions, and current sources represent constant heat flux boundary conditions. Power is input to

the system via the current source Q_{in}. The power generated at Q_{in} can move to any one of the temperature boundary conditions, T_{amb} and $T_{chiller}$.

As was discussed in a previous section, the TED is the most complicated portion of the model. An accurate TEC model must capture Joule heating, as well as Peltier heating and cooling. Thus, a number of independent heat sources is required in the model to fully capture all of the physical phenomena present. It is in the TED sub-model where the parameters derived from metrology are applied to the model. Hence, care must be taken to accurately capture and apply all physical phenomena present. A physical representation of the thermal conductance stack-up of the TED subsystem can be seen in Figure 20. Here, TED is divided into three separate components, the top-side Alumina substrate and interconnects, the TE material, and the bottom-side alumina substrate and interconnects. So that the TED internal temperature can be a solution output in the model, the TE element layer is broken into two separate thermal resistance components.

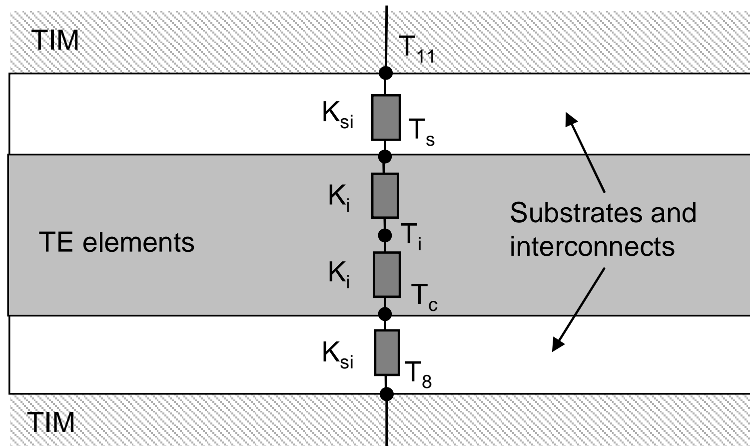

Figure 20-Submodel of the TED system. Representative thermal resistances are overlaid with the physical system layers within the TED.

As can be seen in Figure 20, TED internal conductance components are denoted by the symbol K_i. Equation (34) and equation (35) summarize the calculations to arrive at these parameters.

$$R_i = \frac{R_{th}}{2} \tag{34}$$

$$K_i = \frac{1}{R_i} = \frac{2}{R_{th}} \tag{35}$$

where K_i and R_i are the thermal conductance and resistance of ½ the thickness of the thermoelectric element layer within the TED, respectively. Note that the parameter R_{th} was measured as the thermoelectric element layer thermal resistance, shown previously in Figure 12. Recall that the TED thermal resistance was determined to be a function of temperature of the TED. To simplify the analysis, it will be assumed that only the component R_i of the total has a temperature dependence. As was determined previously, the thermal resistance contribution from the thermoelectric element layer is much larger than that from the alumina substrates. Therefore, if we ignore the temperature dependant thermal resistance due to the alumina substrates, only a slight change in temperature will be ignored, and the corresponding error will be small.

Figure 21 shows the network analogy of the TED sub-model. As can be seen in the figure, there are five sources of heat-flow assumed. These sources are due to the Peltier heating and cooling, as well as Joule heating within the TED. The location at which each source acts can be at either side of the TE elements, or directly at the center of the TE elements. Joule heating is captured by the three terms containing

the square of current. Joule heating can be generated at the top and bottom of the TE elements (arising from an electrical contact resistance), or in the center of the TE elements (arising from a bulk electrical resistance). By allowing the flexibility in the model to distribute the electrical resistance between bulk and contact location, it is possible to examine its effect on the match with experimental data. The sum of electrical contact resistances and bulk electrical resistance must be equal to the total TED resistance. This can be seen in Equation (36).

$$R_j = 2R_{j,c} + R_{j,i} \tag{36}$$

where $R_{j,c}$ is the electrical contact resistance between the TE element layer and interconnects, and $R_{j,i}$ is the bulk electrical resistance of the TE element layer. As was determined from experiment, the TED electrical resistance is a function of temperature. It will be assumed that all temperature dependence of the electrical resistance occurs in the bulk resistance component of the TED.

Aside from the Joule heating, the remaining energy sources are that from Peltier heating and cooling. These terms can also be seen in Figure 21. The Peltier heating and cooling source terms contain the Module Seebeck Coefficient, $\alpha_{p,n}$. These sources are present only at the top and bottom surfaces of the TE elements. This methodology for TED subsystem modeling has been shown to accurately capture the physical behavior [32].

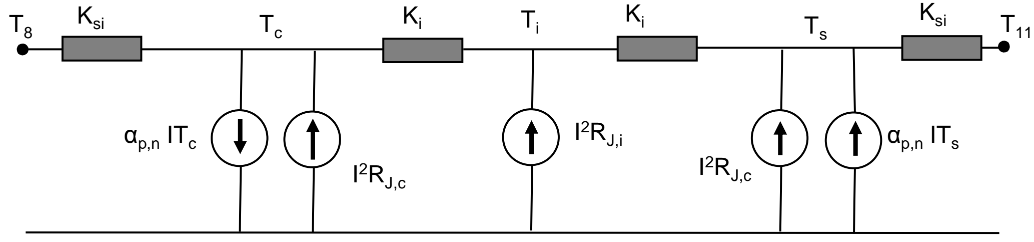

Figure 21-Electrical network schematic of the TED subsystem.

Now that the model has been defined, the next step is to formulate the equations to solve. The system can be reduced to a number of coupled equations, and the number of equations must equal the number of temperature locations for which we desire a solution. Since there are seven system temperatures of interest, there will be seven separate equations which must be simultaneously solved in order to arrive at the solution. Equation (37) through Equation (43) are a result of an energy balance at each system temperature node.

$$(T_{amb} - T_3)K_{loss,bot} + (T_8 - T_3)K_1 + Q_{in} = 0 \tag{37}$$

$$(T_3 - T_8)K_1 + (T_C - T_8)K_{si} = 0 \tag{38}$$

$$(T_8 - T_C)K_{si} + (T_i - T_C)K_i + I^2 R_{j,c} - \alpha_{p,n} I T_C = 0 \tag{39}$$

$$(T_C - T_i)K_i + (T_S - T_i)K_i + I^2 R_{j,i} = 0 \tag{40}$$

$$(T_{11} - T_S)K_{si} + (T_i - T_S)K_i + I^2 R_{j,c} + \alpha_{p,n} I T_S = 0 \tag{41}$$

$$(T_S - T_{11})K_{si} + (T_6 - T_{11})K_1 = 0 \tag{42}$$

$$(T_{amb} - T_6)K_{loss,top} + (T_{11} - T_6)K_1 + (T_{chiller} - T_6)K_{chiller} = 0 \tag{43}$$

Since the parameters $\alpha_{p\text{-}n}$, K_i, and $R_{j,i}$ present in Equation (39), Equation (40), and Equation (41) are all functions of temperature, the solution would normally require

an iterative approach. However, since T_{avg} can be obtained from the metrology output, this information to reduce complexity of the model and compute the temperature-dependant parameters prior to solving the system of equations.

4.2 Modeling Results

A model vs. experiment comparison will be made with locations for which data in both sets are output at the same points in the metrology. Some points in the model cannot be directly compared with experimental data, since they correspond to internal TED temperatures which cannot be measured. Figure 22 shows a schematic of the metrology, with numbered locations for which modeling output will be compared with experimental data (the nomenclature is different from that which was used previously). In Figure 22, locations 1, 2, 6, and 7 will be directly compared with measurement data.

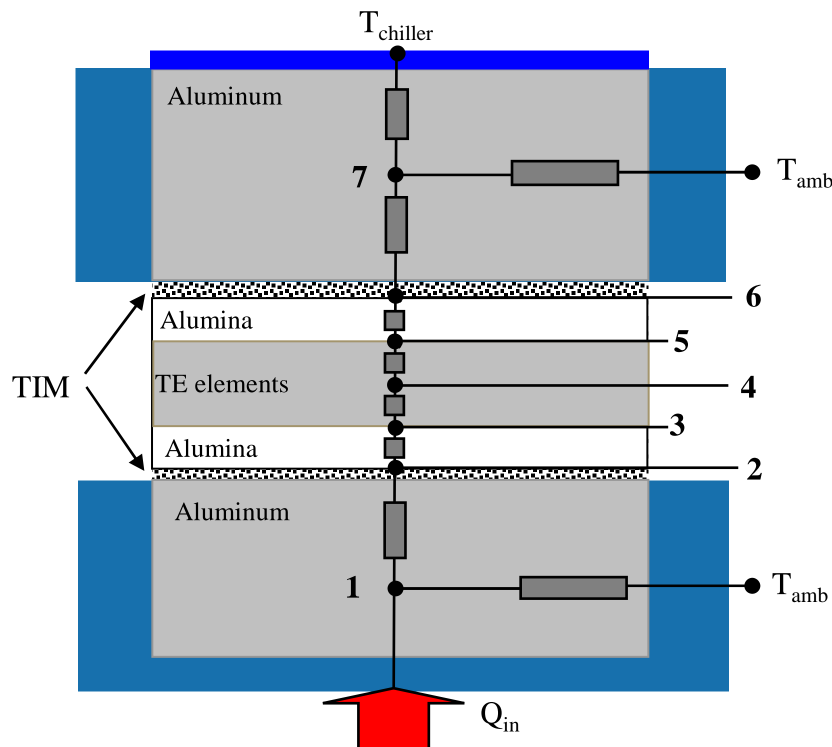

Figure 22-Numbered locations of interest for model matching. Locations 3, 4, and 5 are internal TED temperatures for which no measurement data exists.

Since the thermal loss conductances $K_{loss,top}$ and $K_{loss,bot}$ cannot be directly measured, experimental data must be used to calibrate the model for a baseline case. The case with no TED power can be used to determine the loss conductances by changing the loss conductance until the temperature distribution matches experimental data. Once the values are determined from the baseline calibration, it will be assumed that the values hold for subsequent modeling cases (i.e. cases with applied current to the TED). Figure 23 shows the match of the baseline case, with no TED power. Note that the assumed loss conductance values hold for a large range of temperature, indicating that the convective thermal conductances are not highly temperature dependant.

The calibrated model can be used to evaluate cases with applied TED current. Figures 23 through 27 show the modeling output for the cases with TED current applied. In these cases, all Joule heating is assumed to occur in the center (i.e. $R_{j,c} = 0$). Note that, due to Joule heating, the internal temperature of the TED increases dramatically with current. Since the Joule heating is a quadratic function of the input current, the center temperature increase is more prominent at higher current levels.

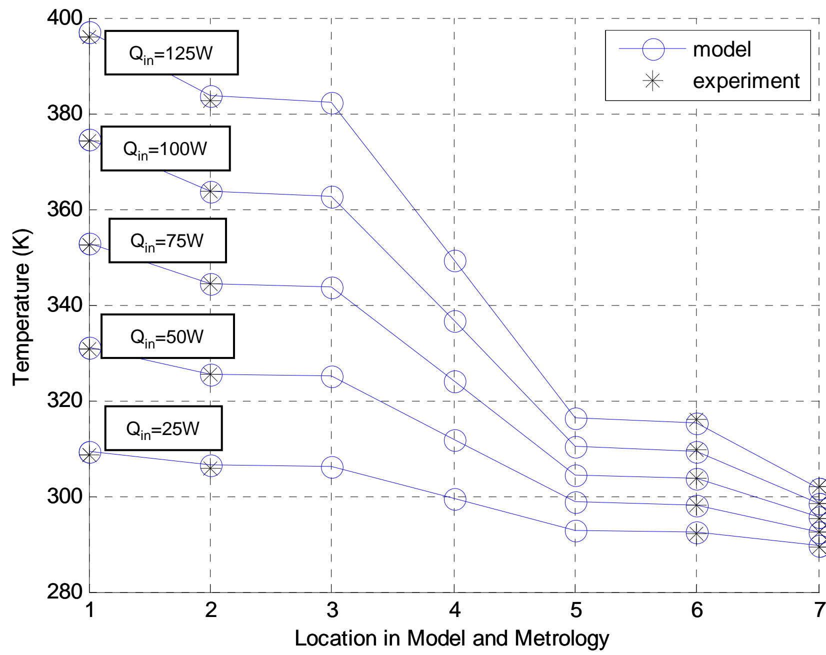

Figure 23-Baseline model calibration case. TEC Current = 0A with various Q_{in}.

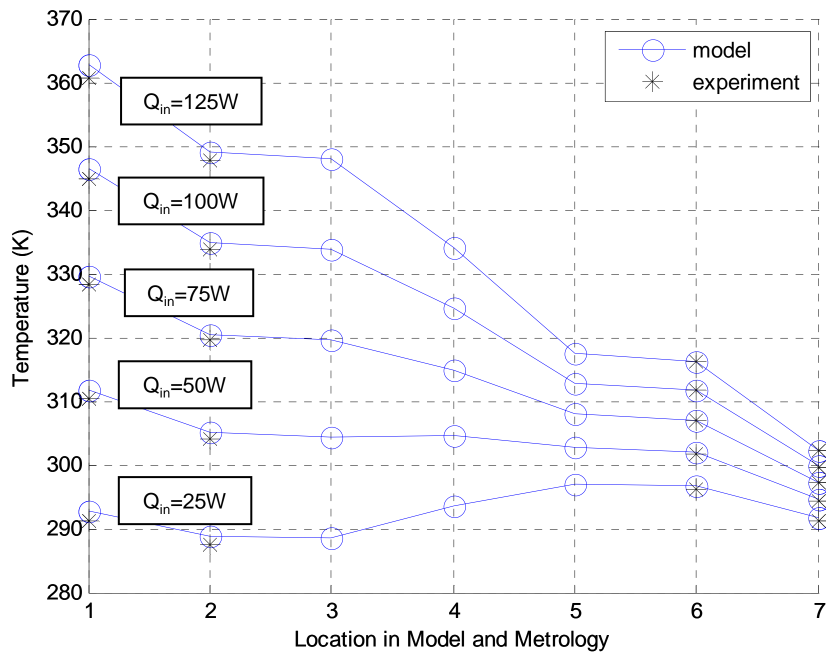

Figure 24-Modeling data plotted with measurements. I = 2A with various Q_{in}.

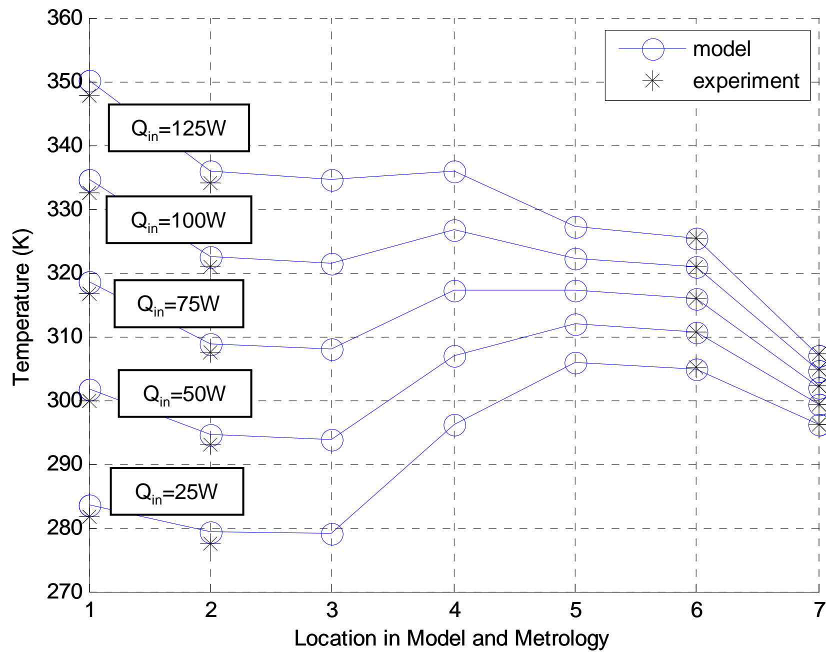

Figure 25-Modeling data plotted with measurements. I = 4A with various Q_{in}.

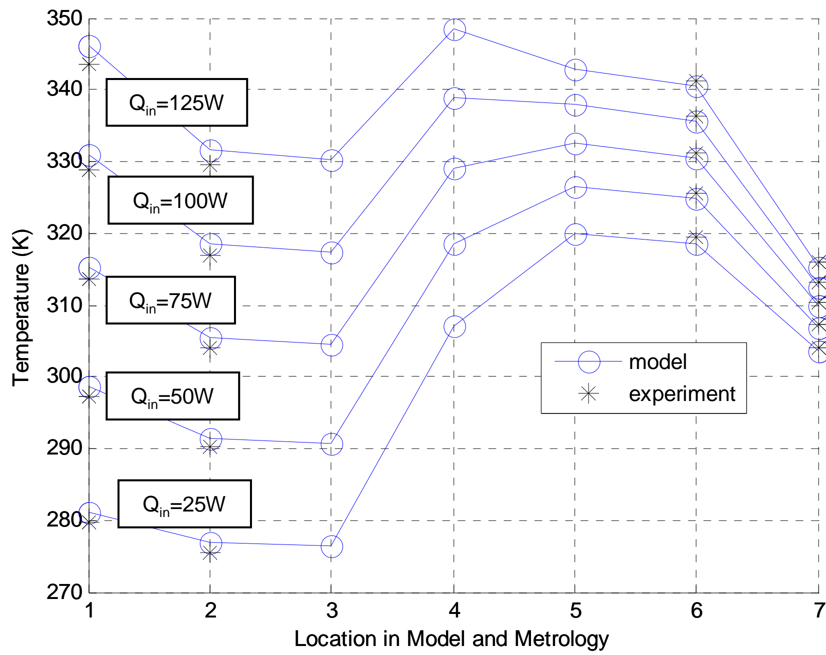

Figure 26-Modeling data plotted with measurements. I = 6A with various Q_{in}.

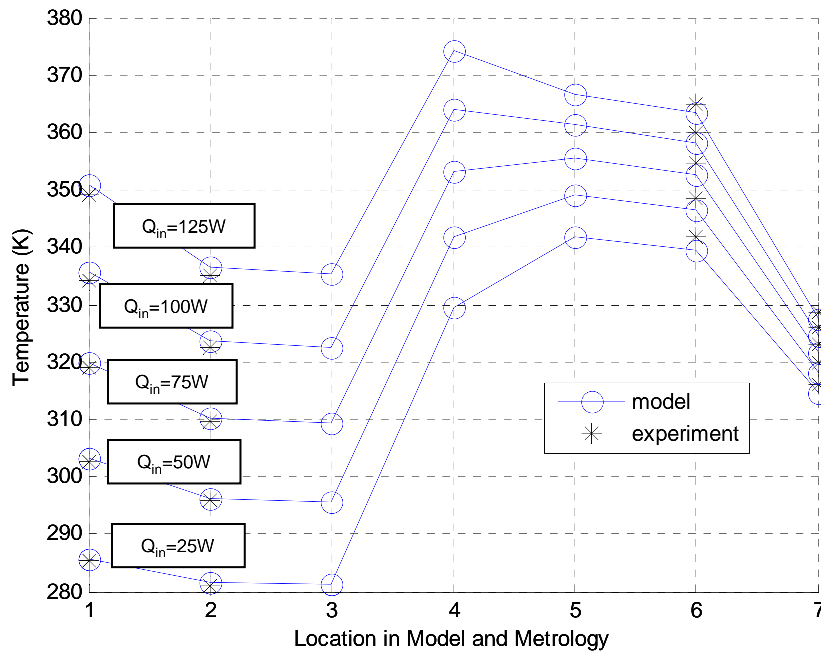

Figure 27-Modeling data plotted with measurements. I = 8A with various Q_{in}.

Note from the Figure 23 though 27 that only four points out of the seven points of interest can be compared to experimental data. This is due to the fact that temperatures internal to the TED cannot be measured. Points 1, 2, 6, and 7 can be used to evaluate the quality of the match between the model and experiment, as these temperatures were those directly measured in the aluminum blocks and at the TED faces (see Figure 8). Though points 3, 4, and 5 cannot be compared with actual measurement, the modeling output for these points demonstrates the power of the predictive thermal model which has been developed, as it would be very difficult to obtain temperatures internal to the TED by direct measurement.

As can be seen in Figure 23 though Figure 27, there is good agreement between model and experimental data. The comparison represents cases with multiple power levels and multiple TED current inputs, thus a very wide range of

operating conditions and temperatures were considered. It is clear that the model captures very well the physics of both the TED and how it interacts with the system. The comparison between the model and experiments shown in figure 23 through figure 27 show that metrology temperatures can be predicted to within 2.5 Kelvin.

Figure 28 and Figure 29 show the power measurement comparisons between model and experiment on the lower aluminum block and upper aluminum blocks, respectively. The data plotted in Figure 28 shows that the TED power input from the control side is in good agreement with experimental conditions. This is a result of good replication in the model of both the power input at the heater and the loss in power from the sides of the lower aluminum block. The match in power on the upper aluminum block, as shown in Figure 29, illustrates that the parasitic power – that from Joule heating and Peltier heating – is fully captured in the model. Thus, the temperature-dependant parameters employed in the model accurately replicate the heat flow coming from the sink side of the TED. The linear fit and R^2 displayed in Figure 28 and Figure 29 show that that the agreement is excellent between heat flow in the model and heat flow in experiment.

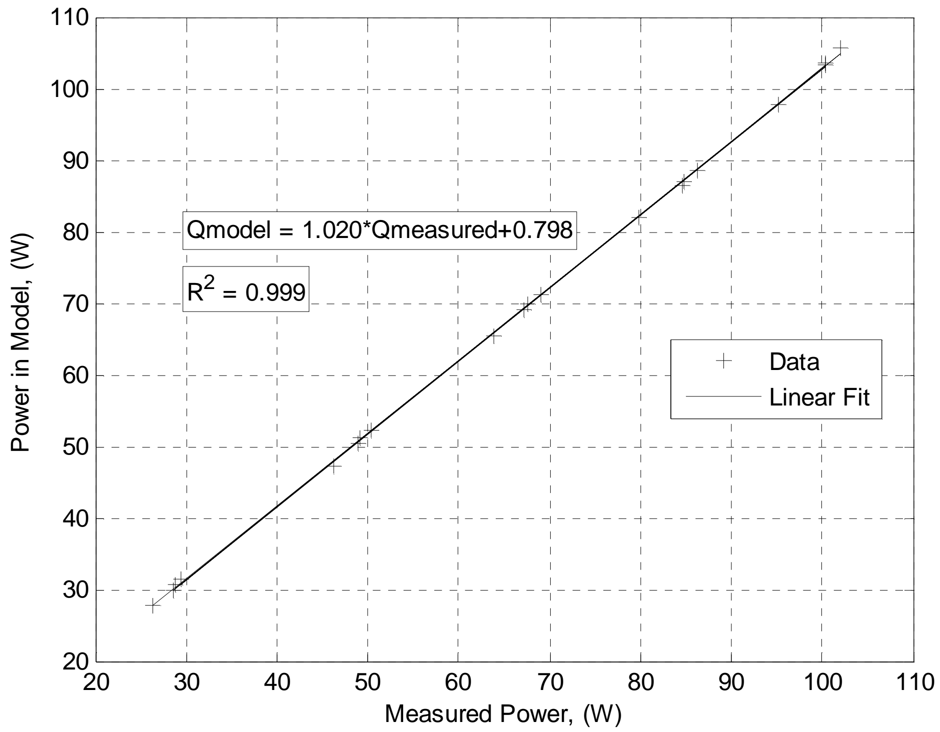

Figure 28-Model vs. Experimental data for power through the lower Al block.

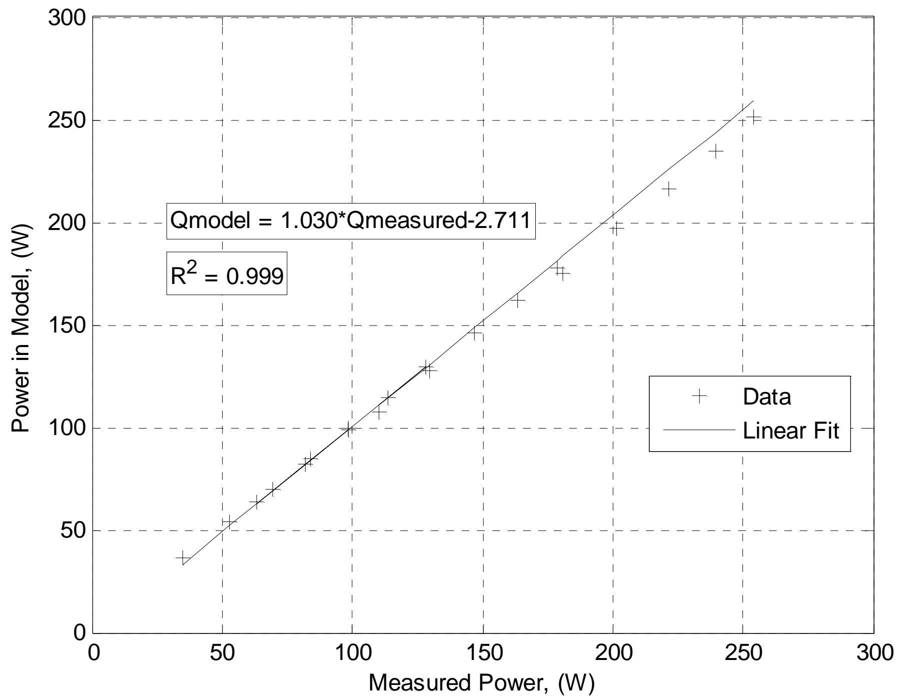

Figure 29-Model vs. Experimental data for power through the upper Al block.

4.3 Buckingham Pi Analysis

To further demonstrate the usefulness of the developed measurement system, a non-dimensional analysis will be included, and experimental data collection used to form a functional relationship between all important terms. A Buckingham Pi Analysis is used to simplify a problem where many inputs can influence an outcome, and where the physical relationship between inputs and outputs is not trivial. By reducing the number of input variables to groups of non-dimensional terms, one is able to vastly reduce the complexity of a problem. Some problems are also too complicated to solve analytically, and a non-dimensional analysis is the only known way to compute a solution – a classic example of this is the problem of computing the pressure drop along a unit length pipeline, due to friction. Correlations have been developed for this problem based on non-dimensional terms, and data has been collected to form the functional relationship. The challenge in such an analysis is the proper formulation of the problem, and also gathering the required data set to form the functional relationship.

A TED system is an ideal candidate for a non-dimensional analysis, since the performance can depend on a number of system-dependant factors, as well as TED-dependant factors. As has been shown, the analytical relationships dictating the performance of a TED (i. e. the cooling, Q_c and the control-side temperature T_c) are dependant on a number of parameters, such as the Module Seebeck Coefficient, the TED electrical resistance, TED thermal resistance, and applied current. System parameters such as the ambient temperature, as well as the sink and control-side thermal resistances (i.e. the thermal resistance from the TED control side to the

device being cooled, as well as the thermal resistance from the TED sink side and the ambient) are all parameters which are necessary to determine the behavior of a TED system. Here, it will be shown that such an analysis can be reduced to only a few non-dimensional terms, and moreover, that developed TED characterization metrology can be easily employed to collect the necessary data to form the relationship between inputs and outputs.

Consider the simplified TED system shown in Figure 31. In the diagram, all main components typical of a TED system have been represented. A very common example of this is in the case of an electronic component which performs optimally at a certain temperature. Often times, such components will generate a quantity of power, which must be removed by the TED. This quantity has been represented in previous equations as the control-side heat flux, Q_c. Such a device would ideally be placed in very close proximity to the control-side of the TED. On the sink side of the TED, there is typically a thermal solution to remove the heat generated by the TED and the device being cooled (the sum of both cold-side heat flow and the power generated by the TED must be removed from the sink-side of the TED). In Figure 31, the sink-side thermal solution is represented by a fan-cooled heat sink attached to the sink-side of the TED with a thermal interface material.

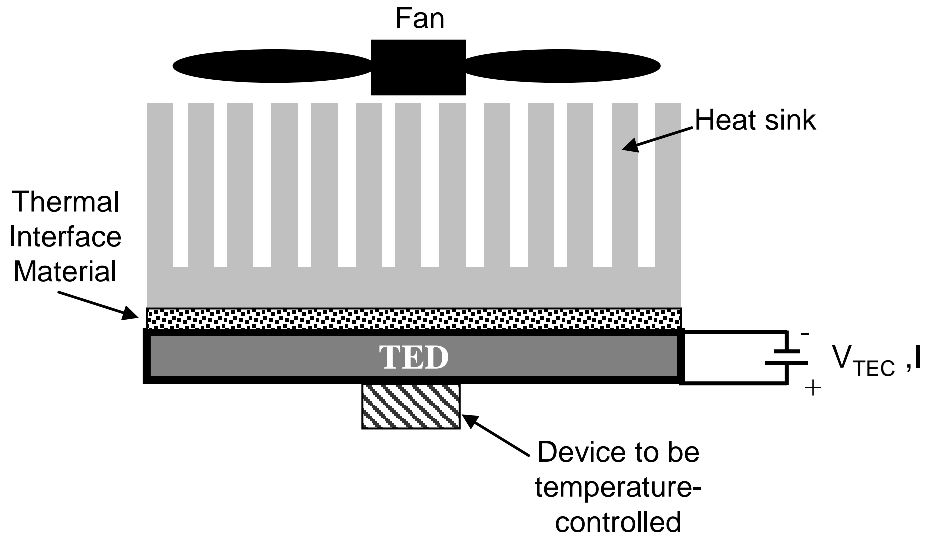

Figure 30-A simple TED system.

An analysis of the physical parameters in the TED system shown in Figure 30 leads to the system shown Figure 31. In this simplified representation, all paths by which power either enters or exits the system are clearly shown. Also shown in Figure 31 are all critical heat flows and temperatures.

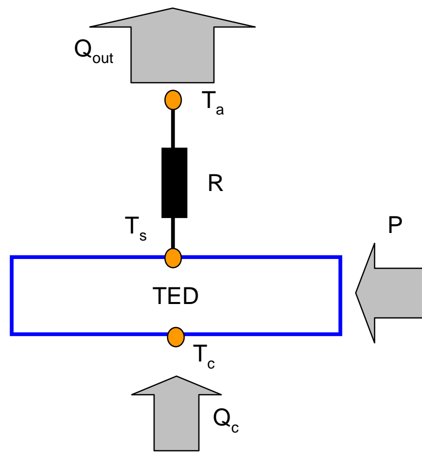

Figure 31-Schematic of a simple TED system, shown with power input and outputs, and associated temperatures.

It is at this point where variables for the Buckinham Pi analysis can be determined. To correctly formulate the problem, any dependant variables must be omitted from the problem formulation First, it is know that the power removed at the sink side of the TED is equal to the Power entering the control side plus the electrical power input to the TED.

$$P_{out} = Q_c + P \tag{44}$$

where P_{out} is the power coming from the sink-side of the TED, and P is the electrical input power to the TED. Here, the parameter P_{out} can be expressed in terms of Q_c and P, and should be removed. Likewise, it is known that the sink-side temperature is a function of the power removed from the sink side of the TED, the sink-side thermal resistance, and the ambient temperature T_a. Thus, T_s, the sink-side temperature, can be removed from the analysis since it can be expressed using other variables.

$$T_s = T_a + R \cdot P_{out} = T_a + R \cdot (Q_c + P) \tag{45}$$

where T_a is the ambient temperature, and R is the TED sink-side thermal resistance to ambient. Since both P_{out} and T_s can be represented by other variables, they must not be included in the analysis. The analysis can be reduced to the system shown in Figure 32.

Equation (46) shows the expected dependant and independent variables.

$$T_c = \phi(Q_c, R, P, T_a) \tag{46}$$

where Φ is the function to be determined using the Buckingham Pi analysis.

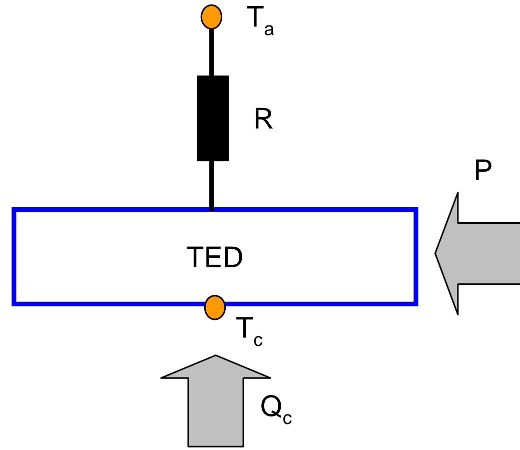

Figure 32-Physical system schematic, shown with only independent variables.

An analysis of the variables in Equation (46) shows that there are only two reference dimensions present, namely temperature (Kelvins), and power (Watts). Thus, based on the Buckingham Pi Theorem, three dimensionless Pi terms are required. A clever selection of the repeating and non-repeating variables yields Equation (47).

$$\frac{T_c}{T_a} = \phi\left(\frac{Q_c}{P}, \frac{RQ_c}{T_a}\right) = \phi\left(COP, \frac{RQ_c}{T_a}\right) \tag{47}$$

where *COP* is the TED coefficient of performance.

Now that the Pi terms are known, the function *Φ* can be determined. To do this, data collected on the TED metrology is employed, since the TED system is conceptually identical to that shown in Figure 30. If a linear equation with two independent variables is assumed, a best-fit equation can be found by performing a least-squares regression. Equation (48) shows the form of the resulting equation.

$$\frac{T_c}{T_a} = 3\times10^{-3} COP + 2.43\left(\frac{RQ_c}{T_a}\right) + 0.91 \tag{48}$$

Figure 33 shows the agreement between the model and data from the metrology. The R^2 of the linear fit is 0.97, the root-mean-square error (RMSE) is 1.3%, and the maximum percent error between the model and experimental data is around 2.3%.

To give the output more practical comparison, both sides of Equation (48) can be multiplied by the ambient temperature to yield the TED control-side temperature. The resulting form can be seen in Equation (49).

$$T_c = 0.9COP + 2.43RQ_c + 273 \qquad (49)$$

Figure 34 shows the corresponding agreement between the TED control-side temperature measured versus that predicted by the model. A contour plot of Equation (48) can be seen in Figure 35. Note that for a fixed $RQ_cT_a^{-1}$, the TED cold-side temperature increases with the COP. This is due to the fact that higher input current causes lower cold-side temperatures, however lower efficiency results since parasitic heat increases proportional to the square of current input. Alternatively, if changes in the values on the x-axis are considered, increases in the value $RQ_cT_a^{-1}$ would imply that operating conditions for the TED get more stringent, (i.e. increases act against better TED performance). Figure 36 shows the contour plot with the TED control-side temperature as the output.

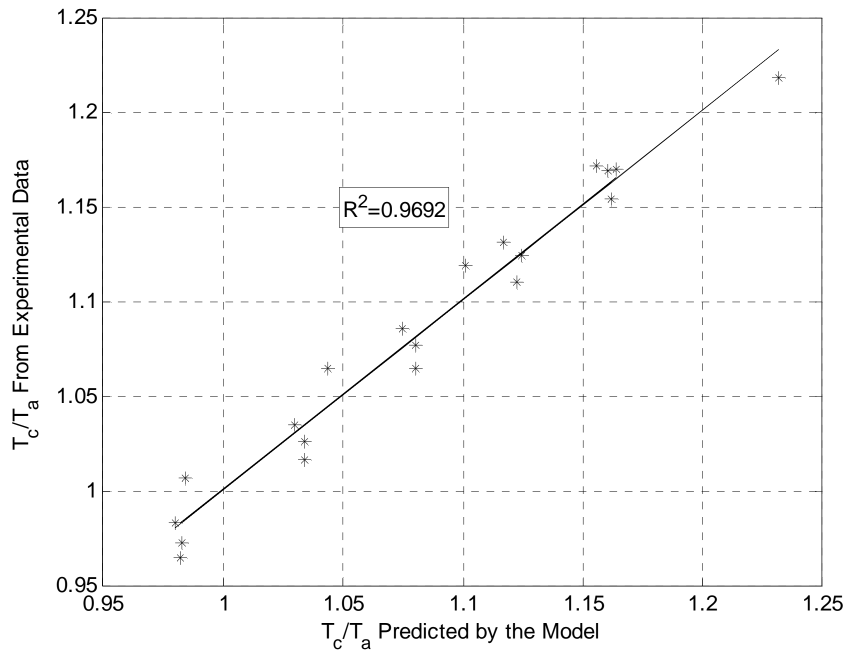

Figure 33-Experimental correlation with that predicted from Equation (48).

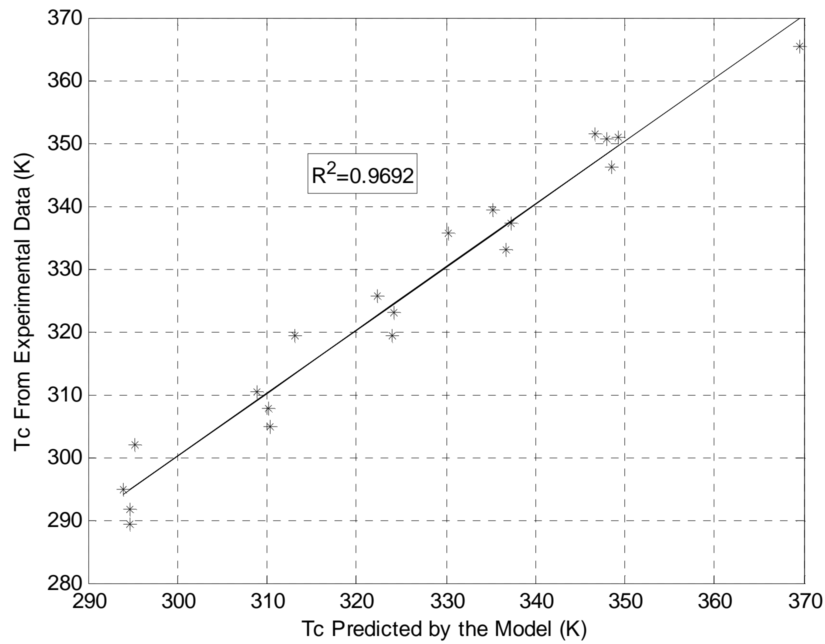

Figure 34-Comparison of TED control versus that from direct measurement, as predicted by Equation (49).

When the relationship is plotted in this form, the practicality of the analysis becomes more evident. For a given ambient temperature, the TED control-side temperature can be estimated based on the COP, control-side heat-flow, and sink-side thermal resistance. This plot can be a great aid to a designer trying to determine the correct TED to use for a specified set of design criteria.

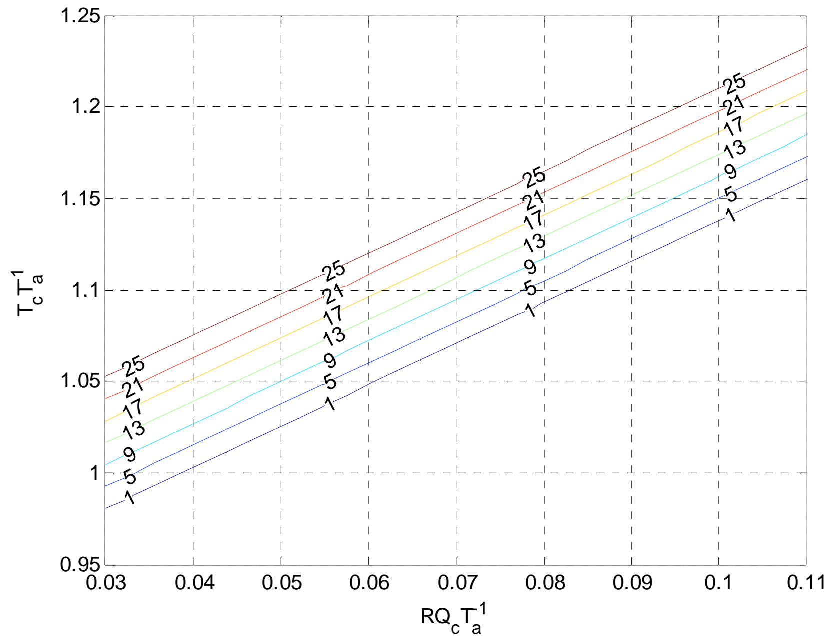

Figure 35-Contour plot of Equation (48). Output $T_cT_a^{-1}$ predicted as a function of the inputs COP and $RQ_cT_a^{-1}$. Lines are labeled and represent constant values of COP.

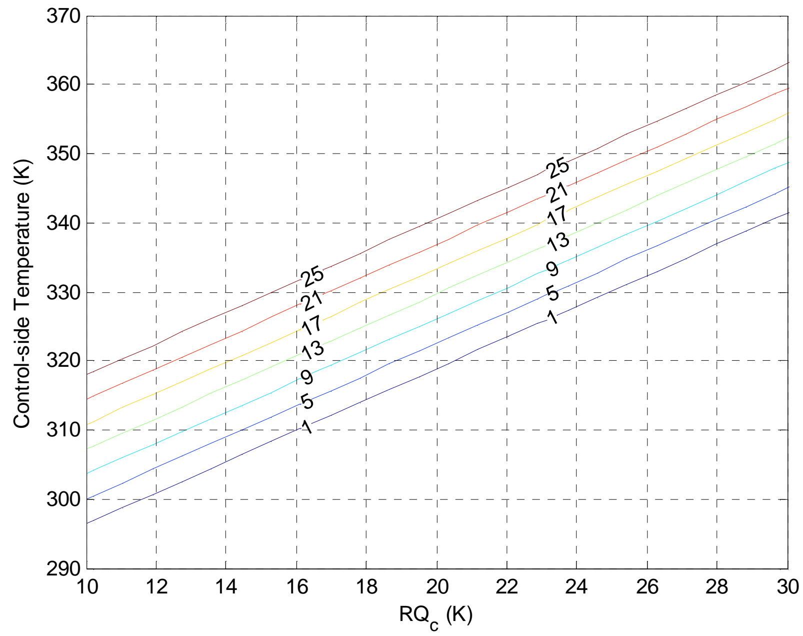

Figure 36-Contour plot of Equation (49). TED Control-side temperature predicted as a function of the inputs COP and RQ_c. Lines are labeled and represent constant values of COP.

5. CONCLUSION

The study of thermoelectric devices represents an area of science which has many opportunities to provide solutions to very challenging problems today. Applications range from energy harvesting and power generation to solid-state refrigeration and thermal management. The subject matter presented here is highly applicable to core development in the area of thermoelectrics, since the accurate characterization of thermoelectrics enables the ability to perform quality control, reliability studies, and most importantly, accurate modeling of TED behavior in a system. This study reviewed TED physics, and highlighted the basic mechanisms which drive TED performance. It was shown that certain physical parameters play leading roles in dictating TED performance, namely the p-type and n-type thermoelectric elements' individual Seebeck Coeficients, electrical resistivity, and thermal conductivity. The fundamental explanation was completed by then extending the analysis to the device-level, where the major components of a TED was reviewed, as well as the fundamental equations describing the device performance. The role which the device plays in scaling the cooling power with the number of TE couples was clearly shown in the equations presented.

A comprehensive review of the most widely used TED metrologies compared advantages and disadvantage of various techniques. The most widely used method for TED characterization, namely, the Transient method, offers many advantages. To name a few, the test is very quick, and provides accurate, repeatable output. Though the technique is ideal for quality control and reliability studies, it does not readily provide the information which is required to fully characterize the TED in a thermal

model. Moreover, the transient technique operates the TED in a regime which is different from actual use-conditions of the TED (i.e. under high input power conditions), which would not allow in-situ reliability investigations. Because manufacturers do not supply the complete set of information which is needed to model the TED, there is a need for a metrology which can readily obtain the information needed to predict TED performance in a thermal system.

The proposed metrology was shown to offer a solution to this problem. Not only can the proposed TED metrology be used to measure all parameters necessary to accurately model a TED, but the system offers the ability to perform an independent validation of the measured parameters. It was shown that the metrology yields very close to the correct conductivity when a sample of copper was measured in place of a TED. Knowing the sample conductivity of the copper, the anticipated temperature difference can be computed. It was shown that the temperature difference was on the order of a few hundredths of one degree K. Thus confidence in the measurements system to yield accurate results was clearly established.

After the validation experiment was concluded, actual measurements on a sample TED were shown. The measurement procedure was demonstrated, reviewing empirical data at each stage, which represents the most efficient, most inclusive strategy for proper characterization of a TED using this metrololgy. All properties, as well as their temperature dependencies are captured in the experiments. The properties measured are then used to compute the parasitic power. Since the metrology allows measurement and computation of the parasitic power independent of the TED parameter measurements, the parasitic power can be

compared to that which is measured and predicted from the derived parameters. Figure 28 and Figures 29 show that the derived parameters do an excellent job of predicting the parasitic power.

In order to offer proof that the measured parameters can accurately predict the TED performance, a system model of the TED and metrology was generated using proven modeling techniques. It was shown that system temperatures could be predicted to within about 2.5K in a thermal network model of the metrology, by using measured parameters directly measured in experiment.

To further demonstrate the advantages of the metrology a non-dimensional analysis was presented. Since the metrology allows such a high range of operating conditions to be imposed on the TED, a comprehensive data set can be used to form the functional relationship in a non-dimensional correlation. It is clear that by performing the analysis, we are able to reduce the complexity by several orders, which can turn a difficult design problem into an extremely trivial exercise.

Overall, the main goal of this thesis is to propose and validate a new and valuable measurement technique for TEDs. As was discussed, the main advantage in the proposed technique is that the output enables accurate modeling TED in a thermal system. Future opportunities within this area of science will heavily depend on the ease by which engineers and scientists can monitor incremental improvements. By improving measurement techniques that enable the ability to fully characterize TEDs, an environment is enabled which fosters technological innovation.

REFERENCES

Biblography

[1] (2008). *U.S Department of Energy: Vehicle Technologies Program*. Available: http://www1.eere.energy.gov/vehiclesandfuels/technologies/engines/solid_state.html

[2] (2011). *Marketwire Inc.: Optical Communication Industry Is Well Positioned for Growth in 2011-2015, Despite Near Term Uncertainty in the Market*. Available: http://www.marketwire.com/press-release/Optical-Communication-Industry-Is-Well-Positioned-Growth-2011-2015-Despite-Near-Term-1418080.htm

[3] *EIC Solutions Inc.: ThermoTEC Series Thermoelectric Air Conditioners*. Available: http://catalog.eicsolutions.com/viewitems/thermoelectric-air-conditioners/2500-btu

[4] *AMS Technologies: Thermoelectric cooling units for laser diode modules - 330W/250W*. Available: http://www.ams.de/de/en/products/detail/id/1853/cat/151/

[5] (2008). *Marlow Indistries, Inc.: Personal Comfort*. Available: http://www.marlow.com/applications/commercial/personal-comfort.html

[6] *Kryotherm TB-127-2.0-1.05*. Available: http://www.kryotherm.com/modulez/down9abc.pdf?filename=/dir2attz/Spec_TB-127-2.0-1.05

[7] (2010). *Nextreme Thermal Solutions: ETEG HV14 Power generator*. Available: http://www.nextreme.com/pages/power_gen/eteg_hv14.shtml

[8] I. Chowdhury*, et al.*, "On-chip cooling by superlattice-based thin-film thermoelectrics," *Nat Nano,* vol. 4, pp. 235-238, 2009.

[9] P. E. Phelan*, et al.*, "Current and future miniature refrigeration cooling technologies for high power microelectronics," *Components and Packaging Technologies, IEEE Transactions on,* vol. 25, pp. 356-365, 2002.

[10] R. Mahajan*, et al.*, "Cooling a Microprocessor Chip," *Proceedings of the IEEE,* vol. 94, pp. 1476-1486, 2006.

[11] R. R. Schaller, "Moore's law: past, present and future," *Spectrum, IEEE,* vol. 34, pp. 52-59, 1997.

[12] J. Williams, "Controlling the temperature of fiber-optic lasers," *EDN,* vol. 46, p. 99, 2001.

[13] *Kryotherm Drift 0.8*. Available: http://www.kryotherm.ru/modulez/down.phtml?filename=/dir2attz/import/Drift-0.8.pdf

[14] J. C. A. Peltier, *Ann. Chem. Phys.,* p. 371, 1834.

[15] D. D. Pollock, "Thermoelectric Phenomena," in *CRC Handbook of Thermoelectrics*, D. M. Rowe, Ed., ed Boca Raton: CRC Press, Inc., 1995, pp. 7-17.

[16] Lasance, "The Seebeck Coefficeint," *Electronics Cooling,* vol. 12, 2006.
[17] H. J. Goldsmid, "Conversion Efficiency and Figure of Merit," in *CRC Handbook of Thermoelectrics*, D. M. Rowe, Ed., ed Boca Raton: CRC Press, Inc., 1995, pp. 19-25.
[18] R. Venkatasubramanian, Siivola, E., Colpitts, T., Brooks, O., "Thin-Film Thermoelectric Devices with High Room Temperature Figures of Merit," *Nature,* vol. 413, pp. 597-602, 2001.
[19] R. J. Buist, "Methodology for Testing Thermoelectric Materials and Devices," in *CRC Handbook of Thermoelectrics*, ed. Boca Raton: CRC Press, Inc., 1995, pp. 189-209.
[20] T. M. Tritt, Ed., *Recent Trends in Thermoelectric Materials Research III* (Semiconductor and Semimetals. San Diego: Academic Press, 2001, p.^pp. Pages.
[21] R. A. Taylor and G. L. Solbrekken, "An Improved Optimization Approach for Thermoelectric Refrigeration Applied to Portable Electronic Equipment," *ASME Conference Proceedings,* vol. 2005, pp. 2139-2145, 2005.
[22] *Kryotherm - TEM Construction*. Available: http://www.kryotherm.ru/index.phtml?tid=87
[23] T. C. Harman and J. M. Honig, *Journal of Applied Physics,* vol. 13, p. 440, 1962.
[24] G. G. Gromov*, et al.*, "Z-Meter: Easy-to-Use Application and Theory," *Proceedings of VI European Workshop on Thermoelectrics,* 2001.
[25] (2011). *RMT. Ltd.* Available: http://www.rmtltd.ru/
[26] D. Mitrani*, et al.*, "Methodology for extracting thermoelectric module parameters," in *Instrumentation and Measurement Technology Conference, 2004. IMTC 04. Proceedings of the 21st IEEE*, 2004, pp. 564-568 Vol.1.
[27] D. Mitrani*, et al.*, "Dynamic measurement system of thermoelectric module parameters," in *Thermoelectrics, 2003 Twenty-Second International Conference on - ICT*, 2003, pp. 524-527.
[28] M. Gao and D. M. Rowe, "A novel principle allowing rapid and accurate measurement of a dimensionless thermoelectric figure of merit," *Measurement Science and Technology,* vol. 12, p. 1261, 2001.
[29] F. N. Masana, "A new approach to the dynamic thermal modelling of semiconductor packages," *Microelectronics Reliability,* vol. 41, pp. 901-912, 2001.
[30] N. Y. A. Shammas*, et al.*, "A simple method for evaluating the transient thermal response of semiconductor devices," *Microelectronics Reliability,* vol. 42, pp. 109-117, 2002.
[31] D. Astrain*, et al.*, "Computational model for refrigerators based on Peltier effect application," *Applied Thermal Engineering,* vol. 25, pp. 3149-3162, 2005.

[32] D. D. L. Wijngaar, *et al.*, "Modelling of Integrated Peltier Elements," in *Technical Proceedings of the 2000 International Conference on Modeling and Simulation of Microsystems*, ed, 2000, pp. 652 - 655.
[33] (2008). *Marlow Indistries, Inc.: Downloads*.
[34] S. R. Annapragada, *et al.*, "Prediction of electrical contact resistivity in thermoelectric modules (TEMs) from module-level measurements," in *Thermal and Thermomechanical Phenomena in Electronic Systems (ITherm), 2010 12th IEEE Intersociety Conference on*, 2010, pp. 1-8.
[35] E. A. Brandes and B. B. Brook, Eds., *Smithells Light Metals Handbook*. Woburn, MA: Reed Eduction and Professional Publishing Ltd, 1998, p.^pp. Pages.
[36] (2011). *eFunda: Conductivity of Copper*. Available: http://www.efunda.com/materials/elements/TC_Table.cfm?Element_ID=Cu
[37] *Omega Engineering: Thermocouples - An Introduction*. Available: http://www.omega.com/thermocouples.html
[38] Y. A. Cengel, *Heat Transfer: A Practical Approach*, 2 ed. Boston: McGraw Hill, 1998.
[39] (2007). *Kryotherm: TEM Contruction*. Available: http://www.kryothermusa.com/indexb848.html?tid=23
[40] H. Scherrer and S. Scherrer, "Bismuth Telluride, Antimony Telluride, and Their Solid Solutions," in *CRC Handbook of Thermoelectrics*, D. M. Rowe, Ed., ed: CRC PRessn, 1995, p. 215.
[41] O. Yamashita and S. Sugihara, "High-performance bismuth-telluride compounds with highly stable thermoelectric figure of merit," *Journal of Materials Science,* vol. 40, pp. 6439-6444, 2005.